Received: 4 February 2022 | Revised: 6 September 2022 | Accepted: 21 September 2022

DOI: 10.1002/nag.3461

RESEARCH ARTICLE

WILEY

Formation and growth of multiple, distinct ice lenses in frost heave

Hao Gao[1] | **Seyed Ali Ghoreishian Amiri**[1] | **Signe Kjelstrup**[2] | **Gustav Grimstad**[1] | **Benoit Loranger**[3] | **Elena Scibilia**[3]

[1]PoreLab, Department of Civil and Environmental Engineering, Norwegian University of Science and Technology (NTNU), Trondheim, Norway

[2]PoreLab, Department of Chemistry, Norwegian University of Science and Technology (NTNU), Trondheim, Norway

[3]Department of Civil and Environmental Engineering, Norwegian University of Science and Technology (NTNU), Trondheim, Norway

Correspondence
Seyed Ali Ghoreishian Amiri, PoreLab, Department of Civil and Environmental Engineering, Norwegian University of Science and Technology (NTNU), Trondheim, Norway.
Email: seyed.amiri@ntnu.no

Abstract

This paper presents a fully coupled thermo-hydro-mechanical (THM) model which simulates frost heave in fully saturated soils. The model is able to simulate the formation and growth of multiple distinct ice lenses. The basic equations of the system were derived using the continuum theory of mixtures, nonequilibrium thermodynamics, and fracture mechanics, considering skeleton deformation, water flow and heat transport. Central to this model is the coupled transport of mass due to the temperature gradient across the frozen fringe, which acts as the main driving force of the phenomenon. The model is formulated in terms of measurable physical properties and thus no ad hoc parametrization is required. In an ice-lens-free state, the system is solved as a continuum using the finite element method (FEM). It is then locally treated as a discontinuous system upon the formation of ice lens, by enriching the elements carrying the embedded ice lens(es) using the extended finite element method (X-FEM). The accuracy and efficiency of the proposed model has been verified using several laboratory tests on Devon silt samples at different overburden pressures and thermal boundary conditions. Shut-off pressures have been also estimated and compared with the experimental results.

KEYWORDS
distinct ice lenses, frost heave, THM coupling, X-FEM

1 | INTRODUCTION

Frost heave refers to the upwards movement of the ground surface caused by the migration of sub-cooled water to a growing ice lens within frost susceptible soils. The phenomenon has been well known for more than a century[1] and is a subject of study in different fields, for example, physics,[2] chemistry,[3] and geotechnical engineering.[4] Various types of theories have been proposed; and a number of experiments, from small-scale one-dimensional tests[5,6] to large-scale three-dimensional cases,[7] have been conducted. The efforts made to model the frost heave may be classified into three different approaches: semi-empirical models,[8–10] phenomenological models,[11–14] and theoretical models.[15–19]

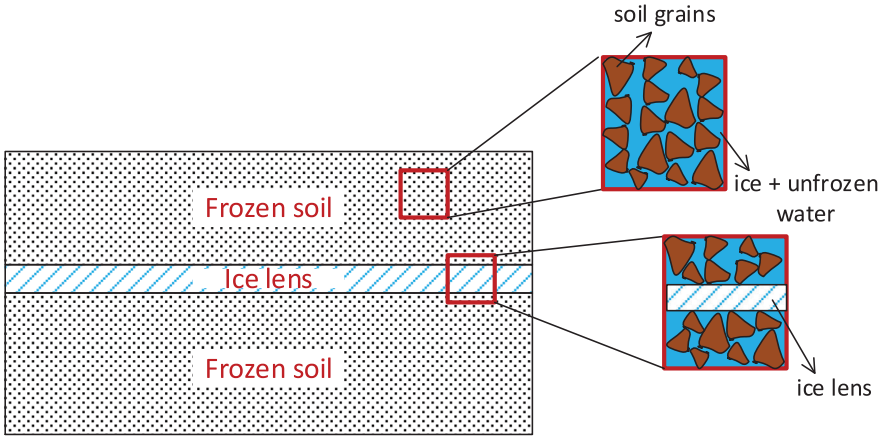

FIGURE 1 A partially frozen soil sample exposed to a temperature gradient: an ice lens is permitted to grow, imposing a material discontinuity in the system

Among the semi-empirical approaches, the segregation potential of Konrad[5,10,20] is widely known by geotechnical engineers. Despite the beauty and simplicity of their model, and the theoretical support provided, the nature of a semi-empirical approach would normally limit its application. For instance, segregation potential cannot be directly used for developing computational tools/models for general purposes.

Phenomenological models, see for example, Ghoreishian Amiri et al.,[13] simulate frost heave through constitutive models that are enriched by a kind of temperature dependent dilatancy. This approach is of high interest among software developers because of its ease of implementation in available computational codes. However, it is not consistent with certain observations regarding the physics of the problem, and thus inconsistent results were observed. For instance, these models predict extremely high suctions (order of MPa) in the unfrozen area of a closed system when subjected to freezing, while experimental measurements report suctions in the order of a few kPas.[21]

Theoretical models, see for example, Rempel[16] and Derjaguin and Churaev,[3] formulate the phenomenon using coupled mass and heat transport equations. This approach is the most precise approach, since it is based on a systematic theory, and can successfully explain the system at different boundary conditions. Few attempts, for example O'Neill and Miller[15] and Thomas et al.,[22] have been made to complement these coupled TH equations by geo-mechanical models in order to explain the dynamics of frost heave phenomenon. They have also numerically solved the system using the FEM. However, the formulation and numerical solution have been developed for continuous systems, while the formation of an ice lens will create material discontinuities inside the porous medium (see Figure 1). The classical FE discretization of such a system might result in unstable solution and normally needs extremely small timesteps in the solution procedure. Indeed, since the ice lens effect is averaged out over the corresponding elements, the results might be mesh dependent.

In this study, the fully coupled THM formulation of Ghoreishian Amiri et al.[23] is modified and tailored to deal with frost heave phenomenon in partially frozen soils. This is done by employing the idea of coupled transport of mass and heat from nonequilibrium thermodynamics, and introducing the latent heat of fusion into the system of equations. The dynamics of the system is formulated according to the conceptual model presented in Ghoreishian Amiri et al.,[19] where the ice lens formation is associated with the appearance of a mechanical crack (grain segregation) in the soil body, and its growth is controlled by the supply of water to the ice lens and the force interaction between the ice lens and the soil body. A very simple segregation criterion (crack criterion) has then been used to find the position for the ice lens to form. As discussed, the solution domain becomes materially discontinuous upon the formation of ice lens. It follows that the continuum formulation has to be integrated over a discontinuous domain using the principle of virtual work. The system of equations is then solved using the X-FE method, which simulates the embedded discontinuities in the elements by enriching the interpolated functions of the FEM. The model is used to simulate a series of frost heave and shut-off pressure tests on Devon silt,[5] and reasonable agreement has been achieved.

2 | GOVERNING EQUATIONS

2.1 | Conservation of linear momentum

Following the derivation of the conservation equations in Ghoreishian Amiri et al.,[23] the linear momentum balance equation is written as:

$$\mathcal{L}^T \boldsymbol{\sigma} - \rho \mathbf{g} = 0 \tag{1}$$

where $\mathbf{g}$ is the gravitational acceleration vector, and $\boldsymbol{\sigma}(= [\sigma_x, \sigma_y, \tau_{xy}]^T)$, ρ and $\mathcal{L}$ are the total stress, total density, and the differential operator, respectively defined:

$$\boldsymbol{\sigma} = \boldsymbol{\sigma}^* + s_w p_w \mathbf{I} \tag{2}$$

$$\rho = (1-n)\rho_s + n s_w \rho_w + n s_i \rho_i \tag{3}$$

$$\mathcal{L} = \begin{bmatrix} \frac{\partial}{\partial x} & 0 & \frac{\partial}{\partial y} \\ 0 & \frac{\partial}{\partial y} & \frac{\partial}{\partial x} \end{bmatrix}^T \tag{4}$$

where $\boldsymbol{\sigma}^*$ is the solid phase stress defined as the combined stress of soil grains and ice,[24] p_w is water pressure, ρ_α and s_α are the density and saturation of the α phase, n is the porosity, and $\mathbf{I}$ is defined as:

$$\mathbf{I} = \begin{bmatrix} 1 & 1 & 0 \end{bmatrix}^T \tag{5}$$

The solid phase stress is considered as the part of the total stress responsible for the mechanical deformation of the system. A simple thermo-elastic constitutive model is assumed here:

$$\dot{\boldsymbol{\sigma}}^* = \mathbf{D}^e (\dot{\boldsymbol{\varepsilon}} - \dot{\boldsymbol{\varepsilon}}_T) \tag{6}$$

where $\mathbf{D}^e$ is the elastic stiffness matrix, $\boldsymbol{\varepsilon}$ ($= [\varepsilon_x, \varepsilon_y, \gamma_{xy}]^T$) is the total strain tensor, and $\boldsymbol{\varepsilon}_T$ denotes the thermal strain, that is defined as:

$$\dot{\boldsymbol{\varepsilon}}_T = -\frac{\mathbf{I}}{3} \beta_s \dot{T} \tag{7}$$

where T is temperature, and β_s is the volumetric thermal expansion coefficient of the skeleton.

The elastic parameters of the system can be computed as[24]:

$$\begin{cases} G = (1-s_i) G_s + s_i G_i \\ K_B = (1-s_i) \frac{(1+e)}{\kappa} p* + s_i K_{Bi} \end{cases} \tag{8}$$

where $G$and K_B are the shear modulus and bulk modulus of the mixture, respectively, G_s and G_i denote the shear modulus of the soil at unfrozen and fully frozen states, respectively, K_{B_i} is the bulk modulus of the system at fully frozen state, $p*$ is the mean solid phase stress and κ is the compressibility of the unfrozen soil.

According to the conceptual model of frost heave introduced by Ghoreishian Amiri et al.,[19] a crack criterion (segregation criterion) is needed to find the initiation and position of the ice lenses. From the physics of the problem, the crack direction can be assumed normal to the temperature gradient, $\mathbf{n}_T$. In this frame, a simple segregation criterion is defined:

$$F = -\sigma^*_{nT} - a = 0 \tag{9}$$

where $\sigma^*_{n_T}$ denotes the normal stress on the plane normal to the temperature gradient, and a is the tensile strength of the soil because of ice cementation, which can be expressed as:

$$a = a_0 - \beta_1 s_i \sigma_{n_T} \tag{10}$$

where a_0 is the tensile strength of the frozen soil at zero overburden/total stress ($\sigma_{n_T} = 0$). These equations reflect the retardation effect of the overburden load on ice lens formation.

2.2 | Conservation of mass

The mass balance equation for the water component can be written as:

$$n\left(\rho_w - \rho_i\right)\dot{s}_w + \nabla^T\left(\rho_w \mathbf{q}_w\right) - \left(s_w\rho_w + s_i\rho_i\right)\dot{\varepsilon}_v + \chi\dot{T} = 0 \tag{11}$$

where $\mathbf{q}_w$ stands for the flux of water, ∇^T indicates the divergence operator, ε_v denotes the volumetric strain and χ is defined as:

$$\chi = ns_w\rho'_{wT} + ns_i\rho'_{iT} + (n-1)\beta_s\left(s_w\rho_w + s_i\rho_i\right) \tag{12}$$

with $\rho'_{wT} = \partial\rho_w/\partial T$ and $\rho'_{iT} = \partial\rho_i/\partial T$.

According to Kjelstrup et al.,[18] the flux of water in a partially frozen soil is affected not only by pressure gradient, but also by temperature gradient, and can be described using the following coupled equation:

$$\mathbf{q}_w = -\frac{k_r K}{\mu_w}(\nabla p_w - \rho_w \mathbf{g}) - \alpha\frac{k_r K}{\mu_w}\frac{\rho_i l}{T}\nabla T \tag{13}$$

where K is the absolute permeability, μ_w is the dynamic viscosity of water, k_r denotes relative permeability for unfrozen water, l is the latent heat of fusion and α is calculated as:

$$\begin{cases} \alpha = 1 - \left(\dfrac{T_0 - T}{T_0 - T_{\mathrm{ff}}}\right) & \mathrm{T_{ff}} < T < T_0 \\ \alpha = 0 & T \geq T_0 \text{ or } \mathrm{T} \leq T_{\mathrm{ff}} \end{cases} \tag{14}$$

where T_0 is the freezing temperature, and T_{ff} is related to the temperature at which an active ice lens stops growing. Equation (14) implies that the coupling term is not active in the unfrozen area, is maximum at the frozen front, and gradually disappears again approaching the fully frozen zone. The word "coupling" is used here to denote the impact of thermal driving force on the mass flux. It is worth noting that the heat flux (see Equation (20) in the next section), is similarly affected by the hydraulic gradient. This is standard in nonequilibrium thermodynamics theory, see Kjelstrup et al.[18] for further references.

Referring to Watanabe and Osada,[25] the relative permeability for unfrozen water can be estimated from that of unsaturated soil using the unfrozen water saturation (s_w). Thus, the model proposed by van Genuchten[26] for estimation of the relative permeability in unsaturated soil, is used here for frozen soil:

$$k_r = \sqrt{s_w}\left[1 - \left(1 - s_w^{1/\lambda}\right)^{\lambda}\right]^2 \tag{15}$$

where λ is a model parameter. The unfrozen water saturation is a function of temperature and is estimated using the soil freezing curve. Referring to Kurylyk and Watanabe,[27] the soil freezing curve can be formulated based on the local pressure difference between ice and water. Considering the Clapeyron equation as the basis for the local pressure difference between ice and water phases, the following mathematical relation can be used[26]:

$$s_w = \left[1 + \left(\frac{S_{cry}}{\rho_r}\right)^{1/(1-\lambda)}\right]^{-\lambda} \tag{16}$$

where ρ_r is a model parameter, and S_{cry} is the local pressure difference between ice and water phase:

$$S_{cry} = p_i - p_w \simeq -\rho_i l \ln \frac{T}{T_0} \tag{17}$$

where p_i is the local ice pressure at the water/ice interface.

Equation (13) plays the main role in the simulation of frost heave, since it contains the main driving force of the phenomenon. According to this equation, when a soil body is subjected to freezing, the temperature gradient term in this equation triggers a transport of water towards the frozen area, but the water flux is, at the same time, limited by the volumetric deformation of the system according to the mass balance Equation (11). Thus, according to the first term in Equation (13), a counter water pressure will be locally built to (partly) cancel the temperature-gradient-induced water flux and balance the total flux with the volumetric deformation of the system. The increase in water pressure will reduce the solid phase stress according to Equation (2), and will finally end up in a tensile crack in the system, according to Equation (9). After that, the temperature-gradient-induced water flux can freely flow towards the segregated zone (crack), where an ice lens is allowed to be built in the system. By further reduction of the temperature, the relative permeability around the ice lens will be dramatically reduced, and the ice lens will stop growing. The same procedure can happen again and initiate new ice lenses.

The proportionality between the water flux and the temperature gradient in frozen soil was shown experimentally by Konrad and Morgenstern[10] through their segregation potential theory. They concluded that the steady state growth rate of the final ice lens is linearly proportional to the temperature gradient in the frozen fringe. It is also theoretically proven by Førland and Kjelstrup Ratkje[28] and Derjaguin and Churaev.[3] In this context, Equation (13) can be considered as a generalization of the previous works that is applicable for both steady state and transient conditions.

2.3 | Conservation of energy

Following the assumptions and procedure in Ghoreishian Amiri et al.,[23] the energy balance equation of the system can be written as:

$$(\rho C)_{\text{eff}} \dot{T} + (\rho_w C_w \mathbf{q}_w) \nabla T + \nabla^T \mathbf{q}_H - l \dot{m}_{w \to i} = 0 \tag{18}$$

where $\rho_\alpha C_\alpha$ is the heat capacity of the α phase, and $(\rho C)_{\text{eff}}$ is the effective heat capacity of the mixture:

$$(\rho C)_{\text{eff}} = (1-n)\rho_s C_s + n s_w \rho_w C_w + n s_i \rho_i C_i \tag{19}$$

and $\mathbf{q}_H$ denote the conductive heat flux, which according to Kjelstrup et al.[18] should be calculated as:

$$\mathbf{q}_H = -\alpha \frac{k_r K}{\mu_w} \rho_i l (\nabla p_w - \rho_w \mathbf{g}) - \left(\lambda_s^{1-n} . \lambda_w^{n s_w} . \lambda_i^{n s_i}\right) \nabla T \tag{20}$$

where λ_α is the is the thermal conductivity of the α phase. The last term in Equation (18) is standing for the phase change energy, where $\dot{m}_{w \to i}$ can be calculated using the mass conservation of the ice phase, without adding any new unknown variable to the system:

$$\dot{m}_{w \to i} = -n \rho_i \dot{s}_w - s_i \rho_i \varepsilon_v - [(1-n) s_i \rho_i \beta_s - n s_i \rho'_{iT}] \dot{T} \tag{21}$$

2.4 | Initial and boundary conditions

Consider a solution domain, Ω, that is bounded by Γ. Initial and boundary conditions, associated with the primary variables, are needed to be defined in order to reach a closed system of equations. The displacement vector $\mathbf{u}$, unfrozen water

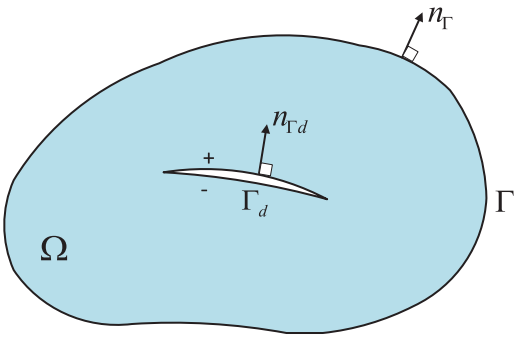

FIGURE 2 The solution domain Ω bounded by Γ and the ice-lens/porous-material interface ($\Gamma_d = \Gamma_d^+ \cup \Gamma_d^-$)

pressure p_w and temperature T are selected as the primary unknown variables of the system. The initial condition has to specify the primary unknown variables at time $t = 0$ on the whole domain:

$$\begin{cases} \mathbf{u} = \mathbf{u}^0 \\ p_w = p_w^0\,, \quad \text{at } t = 0 \text{ and on } \Omega \,\&\, \Gamma \\ T = T^0 \end{cases} \tag{22}$$

Dirichlet boundary conditions are defined by imposing prescribed values of the primary variables:

$$\begin{cases} \mathbf{u} = \bar{\mathbf{u}} & \text{on } \Gamma_u \\ p_w = \bar{p}_w, & \text{on } \Gamma_{p_w} \\ T = \bar{T} & \text{on } \Gamma_T \end{cases} \tag{23}$$

and the prescribed fluxes and tractions would give the Neumann boundary conditions:

$$\begin{cases} \mathbf{l}_\Gamma^T.\boldsymbol{\sigma} = -\bar{\mathbf{t}} & \text{on } \Gamma_{\bar{\mathbf{t}}} \\ \mathbf{q}_w^T \cdot \mathbf{n}_\Gamma = \bar{q}_w, & \text{on } \Gamma_{q_w} \\ \mathbf{q}_H^T \cdot \mathbf{n}_\Gamma = \bar{q}_H & \text{on } \Gamma_{q_H} \end{cases} \tag{24}$$

where $\bar{\mathbf{t}}$, $\bar{q}_w$ and $\bar{q}_H$, respectively, denote the imposed traction, water flux and heat flux, $\mathbf{n}$ is the unit outward normal vector to the boundary:

$$\mathbf{n} = \begin{bmatrix} n_x & n_y \end{bmatrix}^T \tag{25}$$

and the matrix $\mathbf{l}$ is defined as

$$\mathbf{l} = \begin{bmatrix} n_x & 0 & n_y \\ 0 & n_y & n_x \end{bmatrix}^T \tag{26}$$

The conditions $\Gamma_u \cup \Gamma_{\bar{\mathbf{t}}} = \Gamma$, $\Gamma_{p_w} \cup \Gamma_{q_w} = \Gamma$ and $\Gamma_T \cup \Gamma_{q_H} = \Gamma$ should hold on the complementary parts of the boundary.

In the presence of an ice lens, the solution domain will experience material discontinuities, as illustrated in Figure 2. In this case, the ice-lens/porous–material interface, Γ_d ($= \Gamma_d^+ \cup \Gamma_d^-$), can be considered as an internal boundary. The internal boundary conditions can be imposed through mechanical, mass and heat transfer interaction between the ice lens and the surrounding porous medium.

The mechanical interaction comes from the water pressure and ice–soil contact-stress that is acting on the interface. The mass and heat transfer interactions are related to the flux of mass and heat through the interface. Thus, the following

conditions should be fulfilled at the ice-lens/porous-material interface:

$$\begin{cases} \mathbf{l}_{\Gamma_d}^T.\boldsymbol{\sigma} = \mathbf{l}_{\Gamma_d}^T.\left(p_{w_d}\mathbf{I} + \boldsymbol{\sigma}_d^*\right) & \text{on } \Gamma_d \\ -\left[\left[\mathbf{q}_w^T\right]\right]\cdot\mathbf{n}_{\Gamma_d} = \bar{q}_{w_d}, & \text{on } \Gamma_d \\ -\left[\left[\mathbf{q}_H^T\right]\right]\cdot\mathbf{n}_{\Gamma_d} = \bar{q}_{H_d} & \text{on } \Gamma_d \end{cases} \tag{27}$$

where $\bar{q}_{w_d}$ is the net water flow from the porous medium to the ice lens, $\bar{q}_{H_d}$ is the net heat flow from the porous system to the ice lens, $\mathbf{n}_{\Gamma_d}$ is the unit normal vector to the interface, Γ_d, pointing to Ω^+ (see Figure 2), and the notation $[\![\mathbf{q}]\!] = \mathbf{q}^+ - \mathbf{q}^-$ denotes the jump of $\mathbf{q}$ between the two faces of the ice lens. The total stress acting on the interface is distributed between water (p_{w_d}) and ice–soil contact stress (σ_d^*), based on their surface area at the interface. This can be simply formulated as:

$$\frac{\sigma_d^*}{p_{w_d}} = \beta_2 s_{i_d} \tag{28}$$

where s_{i_d} is the ice saturation at the discontinuity, and β_2 is a model parameter.

The first row of Equation (27) is the key ingredient of the model to take the effect of overburden load (total stress, $\boldsymbol{\sigma}$) into account. Upon formation of a crack (segregation), the external load will be partly carried by the unfrozen water phase at the interface of the ice lens and the porous material. Thus, the pressure gradient between the ice-lens/porous-material interface and the water reservoir will increase, which will partly cancel the temperature-gradient-induced water transport towards the ice lens, according to the first term of Equation (13). This mechanism will decrease the growth rate of the ice lens with increasing overburden load.

It is aligned with the experimental observation of Konrad and Morgenstern[29] and Konrad.[30] They concluded the segregation potential and consequently the frost heave rate decrease by increasing overburden pressure. They also stated that the effect of overburden stress on the frost heave rate depends on the soil type and might differ from soil to soil. In the present model the dependency on the material is reflected in Equation (28) through the parameter β_2.

2.5 | Weak form

The coupling between the porous medium and the ice lens might be formulated through the weak form of the governing equations. To this end, in this section, using the virtual work principle, the governing equations are integrated over a discontinuous solution domain introduced in Section 2.4. For the domain of the ice lens, the conservation equations are integrated separately, and introduced as internal boundary conditions to the integral equations of the main domain.

2.5.1 | Conservation of linear momentum

The weak form of the linear momentum balance equation is obtained by integrating the product of Equation (1) and the admissible test function $\delta\mathbf{u}(\mathbf{x}, t)$ over the solution domain Ω, and applying the Divergence theorem:

$$-\int_\Omega \left\{\mathcal{L}\left(\delta\mathbf{u}\right)\right\}^T\boldsymbol{\sigma}d\Omega + \int_{\Gamma_d}\left[\left[\left(\delta\mathbf{u}\right)^T\mathbf{l}_{\Gamma_d}^T.\boldsymbol{\sigma}\right]\right]d\Gamma + \int_\Gamma\left(\delta\mathbf{u}\right)^T\mathbf{l}_\Gamma^T.\boldsymbol{\sigma}d\Gamma - \int_\Omega\left(\delta\mathbf{u}\right)^T\rho\mathbf{g}d\Omega = 0 \tag{29}$$

It must hold for any kinematically admissible test function for displacement, $\delta\mathbf{u}(\mathbf{x}, t)$, satisfying the Dirichlet boundary conditions. Introducing Equation (2), the first row of Equations (24) and (27), and Equation (28) into Equation (29), and assuming traction continuity at the ice-lens/porous-material interface, give:

$$\begin{aligned} &-\int_\Omega\left\{\mathcal{L}\left(\delta\mathbf{u}\right)\right\}^T\boldsymbol{\sigma}^*d\Omega - \int_\Omega\left\{\mathcal{L}\left(\delta\mathbf{u}\right)\right\}^T\left(s_w p_w\mathbf{I}\right)d\Omega \\ &-\int_{\Gamma_d}\left[\left[\left(\delta\mathbf{u}\right)^T\right]\right]\left(\beta_2 s_{i_d}+1\right)\mathbf{l}_{\Gamma_d}^T.\left(p_{wd}\mathbf{I}\right)d\Gamma - \int_{\Gamma_t}\left(\delta\mathbf{u}\right)^T\bar{\mathbf{t}}d\Gamma - \int_\Omega\left(\delta\mathbf{u}\right)^T\rho\mathbf{g}d\Omega = 0 \end{aligned} \tag{30}$$

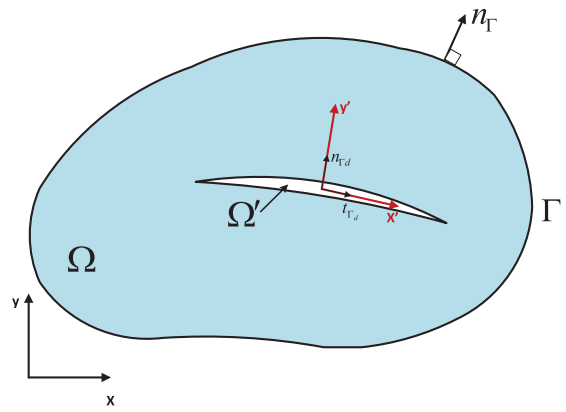

FIGURE 3 The segregated domain and the associated local coordinate system

2.5.2 | Conservation of mass

The weak form of the mass balance equation is obtained by integrating the product of Equation (11) and the admissible test function $\delta p_w(\mathbf{x}, t)$ over the solution domain Ω, and applying the Divergence theorem:

$$\int_\Omega (\delta p_w)\left[n\left(\rho_w-\rho_i\right)\dot{s}_w\right]d\Omega-\int_\Omega\left[\nabla\left(\delta p_w\right)\right]^T\left(\rho_w\mathbf{q}_w\right)d\Omega-\int_{\Gamma_d}\left[\left[\left(\delta p_w\right)\mathbf{q}_w^T\right]\right]\rho_w.\mathbf{n}_{\Gamma_d}d\Gamma$$
$$+\int_{\Gamma_{q_w}}\left(\delta p_w\right)\rho_w\mathbf{q}_w^T.\mathbf{n}_\Gamma d\Gamma-\int_\Omega\left(\delta p_w\right)\left[\left(s_w\rho_w+s_i\rho_i\right)\dot{\varepsilon}_v\right]d\Omega+\int_\Omega\left(\delta p_w\right)\chi\dot{T}d\Omega=0 \tag{31}$$

It must hold for any kinematically admissible test function for (unfrozen) water pressure, $\delta p_w(\mathbf{x}, t)$, satisfying the Dirichlet boundary conditions. Introducing the second row of Equations (24) and (27) into Equation (31), and assuming pressure continuity at the interface:

$$\int_\Omega (\delta p_w)\left[n\left(\rho_w-\rho_i\right)\dot{s}_w\right]d\Omega-\int_\Omega\left[\nabla\left(\delta p_w\right)\right]^T\left(\rho_w\mathbf{q}_w\right)d\Omega+\int_{\Gamma_d}\left(\delta p_w\right)\rho_w\bar{q}_{w_d}d\Gamma$$
$$+\int_{\Gamma_{q_w}}\left(\delta p_w\right)\rho_w\bar{q}_w d\Gamma-\int_\Omega\left(\delta p_w\right)\left[\left(s_w\rho_w+s_i\rho_i\right)\dot{\varepsilon}_v\right]d\Omega+\int_\Omega\left(\delta p_w\right)\chi\dot{T}d\Omega=0 \tag{32}$$

where the third integral in Equation (32) stands for mass transfer between the ice lens and the porous medium. Following the methodology in Mohammadnejad and Khoei,[31] this integral can be calculated by writing the weak form of the mass balance equation of water (and ice) over the segregated domain Ω', as shown in Figure 3:

$$\int_{\Omega'}\left(\delta p_w\right)\left[\left(\rho_w-\rho_i\right)\dot{s}_{w_d}\right]d\Omega-\int_{\Omega'}\left[\nabla\left(\delta p_w\right)\right]^T\left(\rho_w\mathbf{q}_w\right)d\Omega-\int_{\Gamma_d}\left[\delta p_w\right]\rho_w\bar{q}_{w_d}d\Gamma$$
$$-\int_{\Omega'}\left(\delta p_w\right)\left[\left(s_{w_d}\rho_w+s_{i_d}\rho_i\right)\dot{\varepsilon}_{v_d}\right]d\Omega+\int_{\Omega'}\left(\delta p_w\right)\left[s_{w_d}\rho'_{wT}+s_{i_d}\rho'_{iT}\right]\dot{T}d\Omega=0 \tag{33}$$

Equation (33) has been achieved by applying the Divergence theorem and implementing the boundary conditions at the ice-lens/porous-material interface.

Rearranging Equation (33), the mass transfer coupling term is found by calculating the following integrals:

$$\int_{\Gamma_d}\left(\delta p_w\right)\bar{q}_{w_d}d\Gamma=\underbrace{\int_{\Omega'}\left(\delta p_w\right)\left[\left(\rho_w-\rho_i\right)\dot{s}_{w_d}\right]d\Omega}_{\text{IntegralI}}-\underbrace{\int_{\Omega'}\left[\nabla\left(\delta p_w\right)\right]^T\left(\rho_w\mathbf{q}_w\right)d\Omega}_{\text{IntegralII}}$$
$$\underbrace{-\int_{\Omega'}\left(\delta p_w\right)\left[\left(s_{w_d}\rho_w+s_{i_d}\rho_i\right)\dot{\varepsilon}_{v_d}\right]d\Omega}_{\text{IntegralIII}}+\underbrace{\int_{\Omega'}\left(\delta p_w\right)\left[s_{w_d}\rho'_{wT}+s_{i_d}\rho'_{iT}\right]\dot{T}d\Omega}_{\text{IntegralIV}} \tag{34}$$

The integral terms (I)–(IV) over the segregated domain can be approximated in the local coordinate system $(x' - y')$ constructed by the tangential and normal unit vectors to the interface, as shown in Figure 3. Indeed, from the physic of the problem, the crack direction (i.e., x') is assumed normal to the temperature gradient.

Ignoring the variation of water pressure, its corresponding test function, and unfrozen water content over the width of the segregated domain (i.e., in y' direction), the first and second integrals are approximated as:

$$\underbrace{\int_{\Omega'} (\delta p_w) \left[(\rho_w - \rho_i)\, \dot{s}_{w_d}\right] d\Omega}_{\text{IntegralI}} = \int_{\Gamma_d} \int_{-1/2\left[\left[u_{y'}\right]\right]}^{1/2\left[\left[u_{y'}\right]\right]} (\delta p_w) \left[(\rho_w - \rho_i)\, \dot{s}_{w_d}\right] dy' d\Gamma$$

$$= \int_{\Gamma_d} (\delta p_w) \left[\left[u_{y'}\right]\right] \left[(\rho_w - \rho_i)\, \dot{s}_{w_d}\right] d\Gamma \tag{35}$$

$$\underbrace{\int_{\Omega'} \left[\nabla (\delta p_w)\right]^T (\rho_w \mathbf{q}_w)\, d\Omega}_{\text{IntegralII}} = \int_{\Gamma_d} \int_{-1/2\left[\left[u_{y'}\right]\right]}^{1/2\left[\left[u_{y'}\right]\right]} \left(\frac{\partial (\delta p_w)}{\partial x'} q_{w_{x'}} + \frac{\partial (\delta p_w)}{\partial y'} q_{w_{y'}} \right) \rho_w dy' d\Gamma$$

$$= \int_{\Gamma_d} \left(\frac{\partial (\delta p_w)}{\partial x'} q_{w_{x'}} \right) \rho_w \left[\left[u_{y'}\right]\right] d\Gamma \tag{36}$$

where the unfrozen water saturation, and $q_{w_{x'}}$ within the segregated domain are considered as follows:

$$s_{w_d} = \begin{cases} 1 & \text{if } \mathrm{T} > \mathrm{T}_0 \\ s_{w_{\mathrm{res}}} + \dfrac{1 - s_{w_{res}}}{T_0 - T_i} \times (T - T_i) & \text{if } \mathrm{T}_i \le \mathrm{T} \le \mathrm{T}_0 \\ s_{w_{\mathrm{res}}} & \text{if } \mathrm{T} < \mathrm{T}_i \end{cases} \tag{37}$$

$$q_{w_{x'}} = -k_d \left(\frac{\partial p_w}{\partial x'} - \rho_w g_{x'} \right) \tag{38}$$

where T_i is the temperature for the fully frozen state, $s_{w_{\mathrm{res}}}$ is the residual of unfrozen water saturation at temperatures below T_i, and k_d is the hydraulic conductivity of the segregated domain:

$$k_d = s_{w_d} \frac{[\![u]\!]^2}{12\mu_w} \tag{39}$$

Note that there is no thermal coupling term in the mass transport Equation (39), since x' is here defined normal to the temperature gradient.

To approximate the third integral, we assumed that the displacement discontinuity only exists in the normal direction to the ice lens. Therefore, $\varepsilon_{x'_d}$ would be constant over the width of the segregated area (i.e., in y' direction). Thus:

$$\underbrace{\int_{\Omega'} (\delta p_w) \left[\left(s_{w_d}\rho_w + s_{i_d}\rho_i\right) \dot{\varepsilon}_{v_d}\right] d\Omega}_{\text{IntegralIII}} = \int_{\Gamma_d} \int_{-1/2\left[\left[u_{y'}\right]\right]}^{1/2\left[\left[u_{y'}\right]\right]} (\delta p_w) \left(s_{w_d}\rho_w + s_{i_d}\rho_i\right) \left(\dot{\varepsilon}_{x'_d} + \dot{\varepsilon}_{y'_d}\right) dy' d\Gamma =$$

$$\int_{\Gamma_d} (\delta p_w) \left(s_{w_d}\rho_w + s_{i_d}\rho_i\right) \left[\left[u_{y'}\right]\right] \dot{\varepsilon}_{x'_d} d\Gamma - \int_{\Gamma_d} (\delta p_w) \left(s_{w_d}\rho_w + s_{i_d}\rho_i\right) \left[\left[\dot{u}_{y'}\right]\right] d\Gamma \tag{40}$$

Ignoring the variation of temperature over the width of the segregated area, the fourth integral can be approximated as:

$$\underbrace{\int_{\Omega'} (\delta p_w)\left[s_{w_d}\rho'_{wT} + s_{i_d}\rho'_{iT}\right]\dot{T}d\Omega}_{\text{IntegralIV}} = \int_{\Gamma_d}\int_{-1/2\left[\left[u_{y'}\right]\right]}^{1/2\left[\left[u_{y'}\right]\right]} (\delta p_w)\left[s_{w_d}\rho'_{wT} + s_{i_d}\rho'_{iT}\right]\dot{T}dy'd\Gamma$$

$$= \int_{\Gamma_d} (\delta p_w)\left[s_{w_d}\rho'_{wT} + s_{i_d}\rho'_{iT}\right]\dot{T}\left[\left[u_{y'}\right]\right]d\Gamma \tag{41}$$

2.5.3 | Conservation of energy

The weak form of the energy balance equation is obtained by integrating the product of Equation (18) and the admissible test function $\delta T(\mathbf{x}, t)$ over the solution domain Ω, and applying the Divergence theorem:

$$\int_\Omega (\delta T)(\rho C)_{\text{eff}}\dot{T}d\Omega + \int_\Omega (\delta T)\left(\rho_w C_w \mathbf{q}_w^T\right)\nabla T d\Omega - \int_\Omega \left[\nabla(\delta T)\right]^T \mathbf{q}_H d\Omega$$
$$- \int_{\Gamma_d}\left[\left[(\delta T)\mathbf{q}_H^T\right]\right].\mathbf{n}_{\Gamma_d}d\Gamma + \int_{\Gamma_{q_H}}(\delta T)\mathbf{q}_H^T.\mathbf{n}_\Gamma d\Gamma - \int_\Omega (\delta T) l\dot{m}_{w\to i}d\Omega = 0 \tag{42}$$

It must hold for any kinematically admissible test function for temperature, $\delta T(\mathbf{x}, t)$, satisfying the Dirichlet boundary conditions. Introducing the third row of Equations (24) and (27) into Equation (42), and assuming temperature continuity at the ice-lens/porous-media interface:

$$\int_\Omega (\delta T)(\rho C)_{\text{eff}}\dot{T}d\Omega + \int_\Omega (\delta T)\left(\rho_w C_w \mathbf{q}_w^T\right)\nabla T d\Omega - \int_\Omega \left[\nabla(\delta T)\right]^T \mathbf{q}_H d\Omega$$
$$+ \int_{\Gamma_d}(\delta T)\bar{q}_{H_d}d\Gamma + \int_{\Gamma_{q_H}}(\delta T)\bar{q}_H d\Gamma - \int_\Omega (\delta T) l\dot{m}_{w\to i}d\Omega = 0 \tag{43}$$

where the fourth integral stands for heat transfer between the ice lens and the porous system. Similar to the mass transfer coupling, it can be calculated by the weak form of the energy balance equation over the segregated domain Ω':

$$\int_{\Gamma_d}(\delta T)\bar{q}_{H_d}d\Gamma = \underbrace{\int_{\Omega'}(\delta T)(\rho C)_{\text{eff}_d}\dot{T}d\Omega}_{\text{IntegralI}} + \underbrace{\int_{\Omega'}(\delta T)\left(\rho_w C_w \mathbf{q}_w^T\right)\nabla T d\Omega}_{\text{IntegralII}}$$
$$\underbrace{-\int_{\Omega'}\left[\nabla(\delta T)\right]^T \mathbf{q}_H d\Omega}_{\text{IntegralIII}} \underbrace{-\int_{\Omega'}(\delta T) l\left(\dot{m}_{w\to i}\right)_d d\Omega}_{\text{IntegralIV}} \tag{44}$$

where

$$(\rho C)_{\text{eff}_d} = s_{w_d}\rho_w C_w + s_{i_d}\rho_i C_i \tag{45}$$

$$(\dot{m}_{w\to i})_d = -\rho_i \dot{s}_{w_d} - s_{i_d}\rho_i \dot{\varepsilon}_{v_d} + s_{i_d}\rho'_{iT}\dot{T} \tag{46}$$

Note that Equation (46) comes from the mass balance of the ice phase inside the segregated domain. Ignoring the variation of temperature and its corresponding test function over the width of the segregated domain, and following the

procedure in the previous section for $\bar{q}_{w_d}$, the integrals (I)–(IV) in Equation (46) can be approximated as:

$$\underbrace{\int_{\Omega'} (\delta T)(\rho C)_{\text{eff}_d} \frac{D^s T}{Dt} d\Omega}_{\text{IntegralI}} = \int_{\Gamma_d} (\delta T) \left[\!\left[u_{y'}\right]\!\right] (\rho C)_{\text{eff}_d} \dot{T} d\Gamma \tag{47}$$

$$\underbrace{\int_{\Omega'} (\delta T) \left(\rho_w C_w \mathbf{q}_w^T\right) \nabla T d\Omega}_{\text{IntegralII}} = 0 \tag{48}$$

$$\underbrace{\int_{\Omega'} [\nabla (\delta T)]^T \mathbf{q}_H d\Omega}_{\text{IntegralIII}} = 0 \tag{49}$$

$$\underbrace{\int_{\Omega'} (\delta T) l (\dot{m}_{w\to i})_d d\Omega}_{\text{IntegralIV}} = -\int_{\Gamma_d} (\delta T) l \rho_i \left[\!\left[u_{y'}\right]\!\right] \dot{s}_{w_d} d\Gamma - \int_{\Gamma_d} (\delta T) l s_{i_d} \rho_i \left[\!\left[u_{y'}\right]\!\right] \dot{\varepsilon}_{x'_d} d\Gamma$$

$$+ \int_{\Gamma_d} (\delta T) l s_{i_d} \rho_i \left[\!\left[\dot{u}_{y'}\right]\!\right] d\Gamma + \int_{\Gamma_d} (\delta T) s_{i_d} \rho'_{iT} \dot{T} \left[\!\left[u_{y'}\right]\!\right] d\Gamma \tag{50}$$

3 | NUMERICAL SOLUTION

The weak form of the conservation equations of the system obtained in Section 2.5 were discretized in the spatial and time domains using the X-FEM and finite difference method (FDM), respectively. The resulting set of fully coupled and highly nonlinear equations was then solved using the Newton–Raphson procedure.

3.1 | Approximation of the field variables

In order to discretize the integral Equations (30), (32) and (43), the primary unknown variables (i.e., $\mathbf{u}(\mathbf{x}, t)$, $p_w(\mathbf{x}, t)$, $T(\mathbf{x}, t)$) should be approximated using appropriate shape functions. In the proposed X-FEM approach, the ice lens is embedded in the elements and reflected into the numerical solution through discontinuous field variables (or their corresponding fluxes). In this frame, the conventional FEM shape functions are locally enriched using proper enrichment functions to impose the discontinuity of their corresponding field variables (or their corresponding fluxes) at the discontinuity position, Γ_d.

Ice lens growth requires the displacement field normal to the crack direction (i.e., y' direction) to be discontinuous on Γ_d, that is referred to as a strong discontinuity. Indeed, the water and heat flux, in the direction normal to the ice lens, are also discontinuous on Γ_d, while p_w and T are continuous, that is referred to as weak discontinuity. Strong discontinuities can be approximated by adding a discontinuous enrichment function to the corresponding standard approximated space, while weak discontinuities can be simulated using a continuous enrichment function with discontinuous gradient.

3.1.1 | Displacement field

The displacement discontinuity on Γ_d is modelled in this work using a shifted Heaviside function, and the field is approximated as:

$$\mathbf{u}(\mathbf{x}, t) = \sum_{i=1}^{\mathcal{N}} N_{u_i}(\boldsymbol{\xi}) \hat{\mathbf{u}}_i(t) + \sum_{j=1}^{\mathcal{M}} \left[\bar{N}_{u_j}(\boldsymbol{\xi}) \left(H(\varphi(\boldsymbol{\xi})) - H(\varphi(\boldsymbol{\xi}_j))\right) \mathbf{n}_{\Gamma_d}\right] \tilde{u}_j(t) = \mathbf{N}_u^{\text{std}} \hat{\mathbf{u}} + \mathbf{N}_u^{\text{enr}} \mathbf{L} \tilde{\mathbf{u}} \tag{51}$$

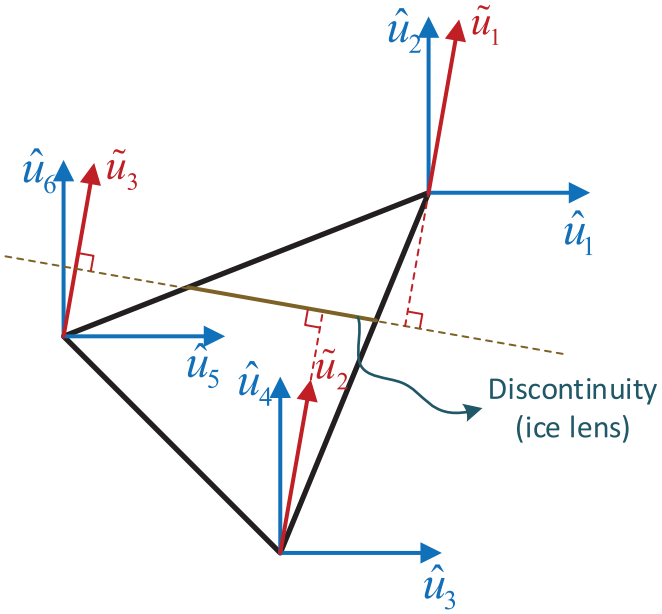

FIGURE 4 Standard and enhanced degrees of freedom for a simple first-order element

where $\boldsymbol{\xi}$ is the position in the local coordinate system of the element, $\mathcal{N}$ is the set of all nodes, $\mathcal{M}$ is the set of enriched nodes, $\mathbf{N}_u(\boldsymbol{\xi})$ and $\bar{\mathbf{N}}_u(\boldsymbol{\xi})$ are the standard FEM shape functions for the displacement field in its standard and enriched parts, respectively, $\hat{\mathbf{u}}$ is the nodal displacement, $\mathbf{L}$ is the transformation matrix between the local direction y' and the global systems (x, y), $\tilde{\mathbf{u}}$ is the enhanced nodal degree of freedom (DOF) parallel to temperature gradient (i.e. normal to the ice lens interface, see Figure 4), and $H(\varphi(\boldsymbol{\xi}))$ is the Heaviside jump function defined as:

$$H(\varphi(\boldsymbol{\xi})) = \begin{cases} +1 & \varphi(\boldsymbol{\xi}) \geq 0 \\ 0 & \varphi(\boldsymbol{\xi}) < 0 \end{cases} \tag{52}$$

and $\varphi(\boldsymbol{\xi})$ is the signed distance function defined based on the absolute value of the level set function:

$$\varphi(\boldsymbol{\xi}) = \left\| \boldsymbol{\xi} - \boldsymbol{\xi}_{\Gamma_d} \right\| \operatorname{sign}\left((\boldsymbol{\xi} - \boldsymbol{\xi}_{\Gamma_d}).\mathbf{n}_{\Gamma_d} \right) \tag{53}$$

where $\boldsymbol{\xi}_{\Gamma_d}$ is the closest point of the embedded discontinuity line (Γ_d), $\|\|$ denotes the Euclidean norm; and accordingly $\|\boldsymbol{\xi} - \boldsymbol{\xi}_{\Gamma_d}\|$ means the distance of point $\boldsymbol{\xi}$ to the embedded discontinuity line (Γ_d).

It is worth noting that using the shifted Heaviside function, the enriched shape function will not affect the adjacent elements, and thus will form the basis for the partition of unity method.[32] Figure 5 shows the aspects of the approximated displacement field for a simple 1D element containing a strong discontinuity.

Similar to Equation (51), the strain vector can be calculated in terms of the standard and enriched nodal values:

$$\boldsymbol{\varepsilon} = -\mathbf{B}_u^{\text{std}}\hat{\mathbf{u}} - \mathbf{B}_u^{\text{enr}}\mathbf{L}\tilde{\mathbf{u}} \tag{54}$$

where $\mathbf{B}_u^{\text{std}}$ $(= \mathcal{L}\mathbf{N}_u^{\text{std}})$ and $\mathbf{B}_u^{\text{enr}}$ $(= \mathcal{L}\mathbf{N}_u^{\text{enr}})$ contain the spatial derivatives of the standard and enriched shape functions, respectively.

Accordingly, the jump in the displacement field in the direction normal to the discontinuity, which gives the thickness of the ice lens thickness, can be calculated as:

$$\left[\left[u_{y'}(\mathbf{x}, t)\right]\right] = u_{y'}(\mathbf{x}^+, t) - u_{y'}(\mathbf{x}^-, t) = \bar{\mathbf{N}}_u\tilde{\mathbf{u}} \tag{55}$$

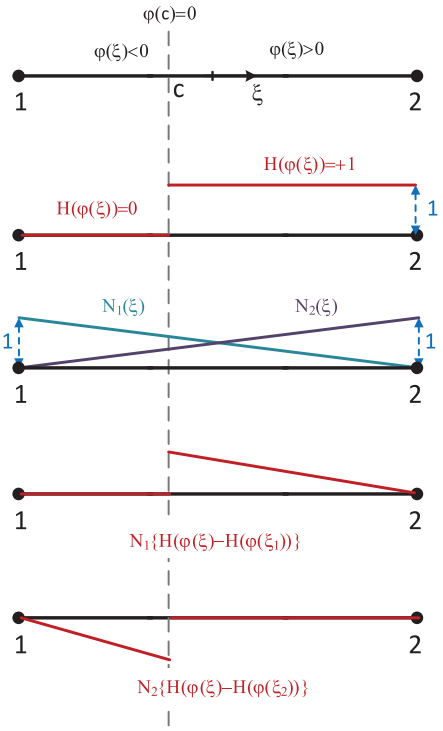

FIGURE 5 Shape and enrichment functions for approximation of the displacement field in a simple first-order 1D element

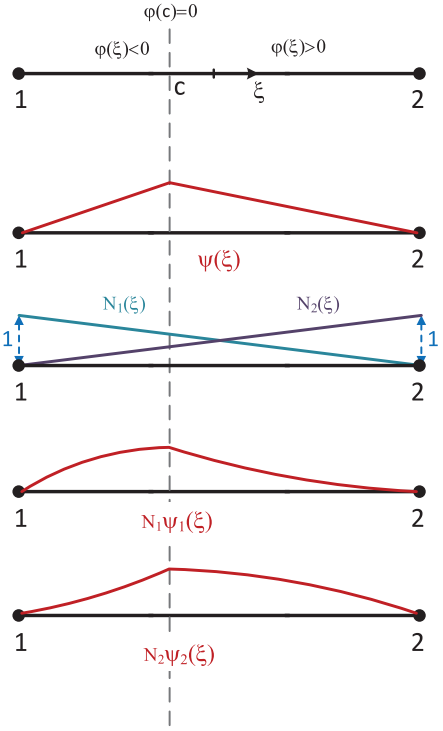

FIGURE 6 Shape and enrichment functions for approximation of the pressure and temperature fields in a simple first-order 1D element

3.1.2 | Pressure and temperature fields

The flux discontinuity on Γ_d is modelled in this work using the modified level-set function proposed by Moës et al.,[33] as shown in Figure 6 for a 1D element. Similar to the shifted Heaviside function, this shape function also fulfills the

requirements for the partition of unity method.

$$p_w(\mathbf{x},t)=\sum_{i=1}^{\mathcal{N}}N_{p_i}(\boldsymbol{\xi})\hat{p}_{w_i}(t)+\sum_{j=1}^{\mathcal{M}}\bar{N}_{p_j}(\boldsymbol{\xi})\psi_p(\boldsymbol{\xi})\tilde{p}_{w_j}(t)=\mathbf{N}_p^{\text{std}}\hat{\mathbf{p}}_w+\mathbf{N}_p^{\text{enr}}\tilde{\mathbf{p}}_w \tag{56}$$

$$T(\mathbf{x},t)=\sum_{i=1}^{\mathcal{N}}N_{T_i}(\boldsymbol{\xi})\hat{T}_i(t)+\sum_{j=1}^{\mathcal{M}}\bar{N}_{T_j}(\boldsymbol{\xi})\psi_T(\boldsymbol{\xi})\tilde{T}_j(t)=\mathbf{N}_T^{\text{std}}\hat{\mathbf{T}}+\mathbf{N}_T^{\text{enr}}\tilde{\mathbf{T}} \tag{57}$$

where $N_p(\boldsymbol{\xi})$ and $N_T(\boldsymbol{\xi})$ are the standard FEM shape functions for the pressure and temperature fields in their standard part, respectively, $\bar{N}_p(\boldsymbol{\xi})$ and $\bar{N}_T(\boldsymbol{\xi})$ are the standard FEM shape functions for pressure and temperature fields in their enriched part, respectively, $\hat{\mathbf{p}}_w$ and $\hat{\mathbf{T}}$ denote the nodal pressure and temperature, respectively, $\tilde{\mathbf{p}}_w$ and $\tilde{\mathbf{T}}$ stand for the enhanced nodal DOFs for pressure and temperature, respectively, and $\psi_\alpha(\boldsymbol{\xi})$ is the modified level-set function given by:

$$\psi_\alpha(\boldsymbol{\xi})=\sum_{i=1}^{\mathcal{M}}\left[\bar{N}_{\alpha_i}(\boldsymbol{\xi})\left|\varphi(\boldsymbol{\xi}_i)\right|\right]-\left|\varphi(\boldsymbol{\xi})\right|\approx\sum_{i=1}^{\mathcal{M}}\bar{N}_{\alpha_i}(\boldsymbol{\xi})\left|\varphi(\boldsymbol{\xi}_i)\right|-\left|\sum_{i=1}^{\mathcal{M}}\bar{N}_{\alpha_i}(\boldsymbol{\xi})\varphi(\boldsymbol{\xi}_i)\right|;\ \alpha=p,T \tag{58}$$

Accordingly, the gradient of the field variables can be calculated in terms of the standard and enriched nodal values:

$$\nabla p_w=\mathbf{B}_p^{\text{std}}\hat{\mathbf{p}}_w+\mathbf{B}_p^{\text{enr}}\tilde{\mathbf{p}}_w \tag{59}$$

$$\nabla T=\mathbf{B}_T^{\text{std}}\hat{\mathbf{T}}+\mathbf{B}_T^{\text{enr}}\tilde{\mathbf{T}} \tag{60}$$

and the jump in the pressure and temperature gradients, in the direction normal to the discontinuity, can be computed as:

$$\left[\!\left[\nabla p_w(\mathbf{x},t).\mathbf{n}_{\Gamma_d}\right]\!\right]=\nabla p_w(\mathbf{x}^+,t).\mathbf{n}_{\Gamma_d}-\nabla p_w(\mathbf{x}^-,t).\mathbf{n}_{\Gamma_d}=-2\bar{\mathbf{N}}_p\tilde{\mathbf{p}}_w \tag{61}$$

$$\left[\!\left[\nabla T(\mathbf{x},t).\mathbf{n}_{\Gamma_d}\right]\!\right]=\nabla T(\mathbf{x}^+,t).\mathbf{n}_{\Gamma_d}-\nabla T(\mathbf{x}^-,t).\mathbf{n}_{\Gamma_d}=-2\bar{\mathbf{N}}_T\tilde{\mathbf{T}} \tag{62}$$

3.2 | Discretization

Following the Bubnov–Galerkin technique, the test functions for displacement $\delta\mathbf{u}$, unfrozen water pressure δp_w and temperature δT in integral Equations (30), (32) and (43) are considered in the same enriched approximating space as their corresponding trial functions, that is, $\mathbf{u}$, p_w and T. Indeed, the weak form of the equations must hold for any kinematically admissible test functions. This will result in the following discretized system:

$$\begin{bmatrix}\mathbf{R}_u^{\text{std}}\\ \mathbf{R}_u^{\text{enr}}\\ \mathbf{R}_p^{\text{std}}\\ \mathbf{R}_p^{\text{enr}}\\ \mathbf{R}_T^{\text{std}}\\ \mathbf{R}_T^{\text{enr}}\end{bmatrix}=\begin{bmatrix}0&0&\mathbf{C}_{up}^{\text{std-std}}&\mathbf{C}_{up}^{\text{std-enr}}&0&0\\ 0&0&\mathbf{C}_{up}^{\text{enr-std}}&\mathbf{C}_{up}^{\text{enr-enr}}&0&0\\ 0&0&\mathbf{Q}_{pp}^{\text{std-std}}&\mathbf{Q}_{pp}^{\text{std-enr}}&\mathbf{C}_{pT}^{\text{std-std}}&\mathbf{C}_{pT}^{\text{std-enr}}\\ 0&0&\mathbf{Q}_{pp}^{\text{enr-std}}&\mathbf{Q}_{pp}^{\text{enr-enr}}&\mathbf{C}_{pT}^{\text{enr-std}}&\mathbf{C}_{pT}^{\text{enr-enr}}\\ 0&0&\mathbf{C}_{Tp}^{\text{std-std}}&\mathbf{C}_{Tp}^{\text{std-enr}}&\mathbf{H}_{TT}^{\text{std-std}}&\mathbf{H}_{TT}^{\text{std-enr}}\\ 0&0&\mathbf{C}_{Tp}^{\text{enr-std}}&\mathbf{C}_{Tp}^{\text{enr-enr}}&\mathbf{H}_{TT}^{\text{enr-std}}&\mathbf{H}_{TT}^{\text{enr-enr}}\end{bmatrix}\begin{bmatrix}\hat{\mathbf{u}}\\ \tilde{\mathbf{u}}\\ \hat{\mathbf{p}}_w\\ \tilde{\mathbf{p}}_w\\ \hat{\mathbf{T}}\\ \tilde{\mathbf{T}}\end{bmatrix}$$

$$+\begin{bmatrix}0&0&0&0&0&0\\ 0&0&0&0&0&0\\ \bar{\mathbf{C}}_{pu}^{\text{std-std}}&\bar{\mathbf{C}}_{pu}^{\text{std-enr}}&0&0&\bar{\mathbf{C}}_{pT}^{\text{std-std}}&\bar{\mathbf{C}}_{pT}^{\text{std-enr}}\\ \bar{\mathbf{C}}_{pu}^{\text{enr-std}}&\bar{\mathbf{C}}_{pu}^{\text{enr-enr}}&0&0&\bar{\mathbf{C}}_{pT}^{\text{enr-std}}&\bar{\mathbf{C}}_{pT}^{\text{enr-enr}}\\ 0&0&0&0&\bar{\mathbf{H}}_{TT}^{\text{std-std}}&\bar{\mathbf{H}}_{TT}^{\text{std-enr}}\\ 0&0&0&0&\bar{\mathbf{H}}_{TT}^{\text{enr-std}}&\bar{\mathbf{H}}_{TT}^{\text{enr-enr}}\end{bmatrix}\begin{bmatrix}\dot{\hat{\mathbf{u}}}\\ \dot{\tilde{\mathbf{u}}}\\ \dot{\hat{\mathbf{p}}}_w\\ \dot{\tilde{\mathbf{p}}}_w\\ \dot{\hat{\mathbf{T}}}\\ \dot{\tilde{\mathbf{T}}}\end{bmatrix}-\begin{bmatrix}{}^{\text{int}}\mathbf{F}_u^{\text{std}}\\ {}^{\text{int}}\mathbf{F}_u^{\text{enr}}\\ {}^{\text{int}}\mathbf{F}_p^{\text{std}}\\ {}^{\text{int}}\mathbf{F}_p^{\text{enr}}\\ {}^{\text{int}}\mathbf{F}_T^{\text{std}}\\ {}^{\text{int}}\mathbf{F}_T^{\text{enr}}\end{bmatrix}-\begin{bmatrix}{}^{\text{ext}}\mathbf{F}_u^{\text{std}}\\ {}^{\text{ext}}\mathbf{F}_u^{\text{enr}}\\ {}^{\text{ext}}\mathbf{F}_p^{\text{std}}\\ {}^{\text{ext}}\mathbf{F}_p^{\text{enr}}\\ {}^{\text{ext}}\mathbf{F}_T^{\text{std}}\\ {}^{\text{ext}}\mathbf{F}_T^{\text{enr}}\end{bmatrix}=0 \tag{63}$$

where the coefficients are summarized in Appendix A.

Equation (63) represents a set of ordinary differential equations in time. The temporal discretization of the system is then performed by the fully implicit first-order accurate finite difference scheme:

$$\begin{bmatrix}\mathbf{R}_u^{\text{std}}\\ \mathbf{R}_u^{\text{enr}}\\ \mathbf{R}_p^{\text{std}}\\ \mathbf{R}_p^{\text{enr}}\\ \mathbf{R}_T^{\text{std}}\\ \mathbf{R}_T^{\text{enr}}\end{bmatrix}_{n+1} = \begin{bmatrix} 0 & 0 & \mathbf{C}_{up}^{\text{std}-\text{std}} & \mathbf{C}_{up}^{\text{std}-\text{enr}} & 0 & 0\\ 0 & 0 & \mathbf{C}_{up}^{\text{enr}-\text{std}} & \mathbf{C}_{up}^{\text{enr}-\text{enr}} & 0 & 0\\ \bar{\mathbf{C}}_{pu}^{\text{std}-\text{std}} & \bar{\mathbf{C}}_{pu}^{\text{std}-\text{enr}} & \Delta t\mathbf{Q}_{pp}^{\text{std}-\text{std}} & \Delta t\mathbf{Q}_{pp}^{\text{std}-\text{enr}} & \bar{\mathbf{C}}_{pT}^{\text{std}-\text{std}}+\Delta t\mathbf{C}_{pT}^{\text{std}-\text{std}} & \bar{\mathbf{C}}_{pT}^{\text{std}-\text{enr}}+\Delta t\mathbf{C}_{pT}^{\text{std}-\text{enr}}\\ \bar{\mathbf{C}}_{pu}^{\text{enr}-\text{std}} & \bar{\mathbf{C}}_{pu}^{\text{enr}-\text{enr}} & \Delta t\mathbf{Q}_{pp}^{\text{enr}-\text{std}} & \Delta t\mathbf{Q}_{pp}^{\text{enr}-\text{enr}} & \bar{\mathbf{C}}_{pT}^{\text{enr}-\text{std}}+\Delta t\mathbf{C}_{pT}^{\text{enr}-\text{std}} & \bar{\mathbf{C}}_{pT}^{\text{enr}-\text{enr}}+\Delta t\mathbf{C}_{pT}^{\text{enr}-\text{enr}}\\ 0 & 0 & \Delta t\mathbf{C}_{Tp}^{\text{std}-\text{std}} & \Delta t\mathbf{C}_{Tp}^{\text{std}-\text{enr}} & \bar{\mathbf{H}}_{TT}^{\text{std}-\text{std}}+\Delta t\mathbf{H}_{TT}^{\text{std}-\text{std}} & \bar{\mathbf{H}}_{TT}^{\text{std}-\text{enr}}+\Delta t\mathbf{H}_{TT}^{\text{std}-\text{enr}}\\ 0 & 0 & \Delta t\mathbf{C}_{Tp}^{\text{enr}-\text{std}} & \Delta t\mathbf{C}_{Tp}^{\text{enr}-\text{enr}} & \bar{\mathbf{H}}_{TT}^{\text{enr}-\text{std}}+\Delta t\mathbf{H}_{TT}^{\text{enr}-\text{std}} & \bar{\mathbf{H}}_{TT}^{\text{enr}-\text{enr}}+\Delta t\mathbf{H}_{TT}^{\text{enr}-\text{enr}} \end{bmatrix}_{n+1}\begin{bmatrix}\hat{\mathbf{u}}\\ \tilde{\mathbf{u}}\\ \hat{\mathbf{p}}_w\\ \tilde{\mathbf{p}}_w\\ \hat{\mathbf{T}}\\ \tilde{\mathbf{T}}\end{bmatrix}_{n+1}$$

$$-\begin{bmatrix}{}^{\text{int}}\mathbf{F}_u^{\text{std}}\\ {}^{\text{int}}\mathbf{F}_u^{\text{enr}}\\ \Delta t^{\text{int}}\mathbf{F}_p^{\text{std}}\\ \Delta t^{\text{int}}\mathbf{F}_p^{\text{enr}}\\ \Delta t^{\text{int}}\mathbf{F}_T^{\text{std}}\\ \Delta t^{\text{int}}\mathbf{F}_T^{\text{enr}}\end{bmatrix}_{n+1} - \begin{bmatrix}{}^{\text{ext}}\mathbf{F}_u^{\text{std}}\\ {}^{\text{ext}}\mathbf{F}_u^{\text{enr}}\\ \Delta t^{\text{ext}}\mathbf{F}_p^{\text{std}}\\ \Delta t^{\text{ext}}\mathbf{F}_p^{\text{enr}}\\ \Delta t^{\text{ext}}\mathbf{F}_T^{\text{std}}\\ \Delta t^{\text{ext}}\mathbf{F}_T^{\text{enr}}\end{bmatrix}_{n+1} - \begin{bmatrix} 0 & 0 & 0 & 0 & 0 & 0\\ 0 & 0 & 0 & 0 & 0 & 0\\ \bar{\mathbf{C}}_{pu}^{\text{std}-\text{std}} & \bar{\mathbf{C}}_{pu}^{\text{std}-\text{enr}} & 0 & 0 & \bar{\mathbf{C}}_{pT}^{\text{std}-\text{std}} & \bar{\mathbf{C}}_{pT}^{\text{std}-\text{enr}}\\ \bar{\mathbf{C}}_{pu}^{\text{enr}-\text{std}} & \bar{\mathbf{C}}_{pu}^{\text{enr}-\text{enr}} & 0 & 0 & \bar{\mathbf{C}}_{pT}^{\text{enr}-\text{std}} & \bar{\mathbf{C}}_{pT}^{\text{enr}-\text{enr}}\\ 0 & 0 & 0 & 0 & \bar{\mathbf{H}}_{TT}^{\text{std}-\text{std}} & \bar{\mathbf{H}}_{TT}^{\text{std}-\text{enr}}\\ 0 & 0 & 0 & 0 & \bar{\mathbf{H}}_{TT}^{\text{enr}-\text{std}} & \bar{\mathbf{H}}_{TT}^{\text{enr}-\text{enr}}\end{bmatrix}_{n+1}\begin{bmatrix}\hat{\mathbf{u}}\\ \tilde{\mathbf{u}}\\ \hat{\mathbf{p}}_w\\ \tilde{\mathbf{p}}_w\\ \hat{\mathbf{T}}\\ \tilde{\mathbf{T}}\end{bmatrix}_{n} = 0 \tag{64}$$

where $\Delta t = t_{n+1} - t_n$ is the time step increment, and the subscripts n and $n+1$ denote time steps.

3.3 | Linearization and solution strategy

Equation (64) represents a set of highly nonlinear equations. Linearization is then performed using the Newton–Raphson method. Expanding Equation (64) with the first-order truncated Taylor-series results in the following linear approximation:

$$\mathbf{J}_{n+1}^{i}\begin{bmatrix}\Delta\hat{\mathbf{u}}\\ \Delta\tilde{\mathbf{u}}\\ \Delta\hat{\mathbf{p}}_w\\ \Delta\tilde{\mathbf{p}}_w\\ \Delta\hat{\mathbf{T}}\\ \Delta\tilde{\mathbf{T}}\end{bmatrix}_{n+1}^{i+1} = -\begin{bmatrix}\mathbf{R}_u^{\text{std}}\\ \mathbf{R}_u^{\text{enr}}\\ \mathbf{R}_p^{\text{std}}\\ \mathbf{R}_p^{\text{enr}}\\ \mathbf{R}_T^{\text{std}}\\ \mathbf{R}_T^{\text{enr}}\end{bmatrix}_{n+1}^{i} \tag{65}$$

where the superscripts denote iterations, $\mathbf{R}$ is the residual vector, and $\mathbf{J}$ is the Jacobian matrix:

$$\mathbf{J} = \begin{bmatrix} \frac{\partial\mathbf{R}_u^{\text{std}}}{\partial\hat{\mathbf{u}}} & \frac{\partial\mathbf{R}_u^{\text{std}}}{\partial\tilde{\mathbf{u}}} & \frac{\partial\mathbf{R}_u^{\text{std}}}{\partial\hat{\mathbf{p}}_w} & \frac{\partial\mathbf{R}_u^{\text{std}}}{\partial\tilde{\mathbf{p}}_w} & \frac{\partial\mathbf{R}_u^{\text{std}}}{\partial\hat{\mathbf{T}}} & \frac{\partial\mathbf{R}_u^{\text{std}}}{\partial\tilde{\mathbf{T}}}\\ \frac{\partial\mathbf{R}_u^{\text{enr}}}{\partial\hat{\mathbf{u}}} & \frac{\partial\mathbf{R}_u^{\text{enr}}}{\partial\tilde{\mathbf{u}}} & \frac{\partial\mathbf{R}_u^{\text{enr}}}{\partial\hat{\mathbf{p}}_w} & \frac{\partial\mathbf{R}_u^{\text{enr}}}{\partial\tilde{\mathbf{p}}_w} & \frac{\partial\mathbf{R}_u^{\text{enr}}}{\partial\hat{\mathbf{T}}} & \frac{\partial\mathbf{R}_u^{\text{enr}}}{\partial\tilde{\mathbf{T}}}\\ \frac{\partial\mathbf{R}_p^{\text{std}}}{\partial\hat{\mathbf{u}}} & \frac{\partial\mathbf{R}_p^{\text{std}}}{\partial\tilde{\mathbf{u}}} & \frac{\partial\mathbf{R}_p^{\text{std}}}{\partial\hat{\mathbf{p}}_w} & \frac{\partial\mathbf{R}_p^{\text{std}}}{\partial\tilde{\mathbf{p}}_w} & \frac{\partial\mathbf{R}_p^{\text{std}}}{\partial\hat{\mathbf{T}}} & \frac{\partial\mathbf{R}_p^{\text{std}}}{\partial\tilde{\mathbf{T}}}\\ \frac{\partial\mathbf{R}_p^{\text{enr}}}{\partial\hat{\mathbf{u}}} & \frac{\partial\mathbf{R}_p^{\text{enr}}}{\partial\tilde{\mathbf{u}}} & \frac{\partial\mathbf{R}_p^{\text{enr}}}{\partial\hat{\mathbf{p}}_w} & \frac{\partial\mathbf{R}_p^{\text{enr}}}{\partial\tilde{\mathbf{p}}_w} & \frac{\partial\mathbf{R}_p^{\text{enr}}}{\partial\hat{\mathbf{T}}} & \frac{\partial\mathbf{R}_p^{\text{enr}}}{\partial\tilde{\mathbf{T}}}\\ \frac{\partial\mathbf{R}_T^{\text{std}}}{\partial\hat{\mathbf{u}}} & \frac{\partial\mathbf{R}_T^{\text{std}}}{\partial\tilde{\mathbf{u}}} & \frac{\partial\mathbf{R}_T^{\text{std}}}{\partial\hat{\mathbf{p}}_w} & \frac{\partial\mathbf{R}_T^{\text{std}}}{\partial\tilde{\mathbf{p}}_w} & \frac{\partial\mathbf{R}_T^{\text{std}}}{\partial\hat{\mathbf{T}}} & \frac{\partial\mathbf{R}_T^{\text{std}}}{\partial\tilde{\mathbf{T}}}\\ \frac{\partial\mathbf{R}_T^{\text{enr}}}{\partial\hat{\mathbf{u}}} & \frac{\partial\mathbf{R}_T^{\text{enr}}}{\partial\tilde{\mathbf{u}}} & \frac{\partial\mathbf{R}_T^{\text{enr}}}{\partial\hat{\mathbf{p}}_w} & \frac{\partial\mathbf{R}_T^{\text{enr}}}{\partial\tilde{\mathbf{p}}_w} & \frac{\partial\mathbf{R}_T^{\text{enr}}}{\partial\hat{\mathbf{T}}} & \frac{\partial\mathbf{R}_T^{\text{enr}}}{\partial\tilde{\mathbf{T}}} \end{bmatrix} \tag{66}$$

Solving the linear system in Equation (65) in each iteration gives the increment of the nodal DOF, and the corresponding nodal values will then be updated as:

$$\begin{bmatrix} \hat{\mathbf{u}} \\ \tilde{\mathbf{u}} \\ \hat{\mathbf{p}}_w \\ \tilde{\mathbf{p}}_w \\ \hat{\mathbf{T}} \\ \tilde{\mathbf{T}} \end{bmatrix}_{n+1}^{i+1} = \begin{bmatrix} \hat{\mathbf{u}} \\ \tilde{\mathbf{u}} \\ \hat{\mathbf{p}}_w \\ \tilde{\mathbf{p}}_w \\ \hat{\mathbf{T}} \\ \tilde{\mathbf{T}} \end{bmatrix}_{n+1}^{i} + \begin{bmatrix} \Delta\hat{\mathbf{u}} \\ \Delta\tilde{\mathbf{u}} \\ \Delta\hat{\mathbf{p}}_w \\ \Delta\tilde{\mathbf{p}}_w \\ \Delta\hat{\mathbf{T}} \\ \Delta\tilde{\mathbf{T}} \end{bmatrix}_{n+1}^{i+1} \tag{67}$$

The iterative procedure will continue to vanish the residual vector, $\mathbf{R}$, within a certain tolerance.

4 | MODEL VALIDATION

A set of frost heave tests and shut-off pressure estimations conducted by Konrad[5] on Devon silt, are used to verify the model. Devon silt is a well characterized soil with reliable test data and reports. Most of the model parameters including hydraulic and thermal conductivities, are directly obtained from the available reports, for example, Azmatch.[34] The samples were prepared from slurries at a moisture content of about 50% to 60%; and consolidated to 210 kPa in three stages. After consolidation, a water content of 27% to 30% was reported; it was relatively uniform throughout the specimen. The model parameters for Devon silt are listed in Table 1.

TABLE 1 Devon silt properties

Water density (ton/m^3)	$\rho_w = 1$
Ice density (ton/m^3)	$\rho_i = 0.9$
Soil density (ton/m^3)	$\rho_s = 2.6$
Initial porosity (%)	$n = 38$
Absolute permeability (m^2)	$K = 1.5 \times 10^{-16}$
Water viscosity (kPa s)	$\mu_w = 1.5 \times 10^{-6}$
Relative permeability parameter	$\lambda = 0.38$
Soil freezing curve parameter (kPa)	$\rho_r = 15$
Specific heat capacity of water (kJ/ton K)	$C_w = 4190$
Specific heat capacity of ice (kJ/ton K)	$C_i = 2095$
Specific heat capacity of soil (kJ/ton K)	$C_s = 900$
Thermal conductivity of water (W/m K)	$\lambda_w = 0.6$
Thermal conductivity of ice (W/m K)	$\lambda_i = 2.2$
Thermal conductivity of soil (W/m K)	$\lambda_s = 3$
Latent heat of fusion (kJ/kg)	$l = 334$
Freezing temperature (K)	$T_0 = 273.16$
Minimum temperature for ice lens growth (K)	$T_{\mathrm{ff}} = 269.16$
Maximum ice lens temperature at fully frozen state (K)	$T_i = 273$
Residual unfrozen water saturation in ice lens interface (%)	$s_{w_{\mathrm{res}}} = 2$
Oedometer modulus at fully frozen sate (GPa)	$K_{B_i} = 0.2$
Soil compressibility	$\kappa = 3 \times 10^{-4}$
Tensile strength at zero overburden (kPa)	$a_0 = 8$
Variation of tensile strength with overburden	$\beta_1 = 2.1$
Mechanical parameter for ice lens interface	$\beta_2 = 20$

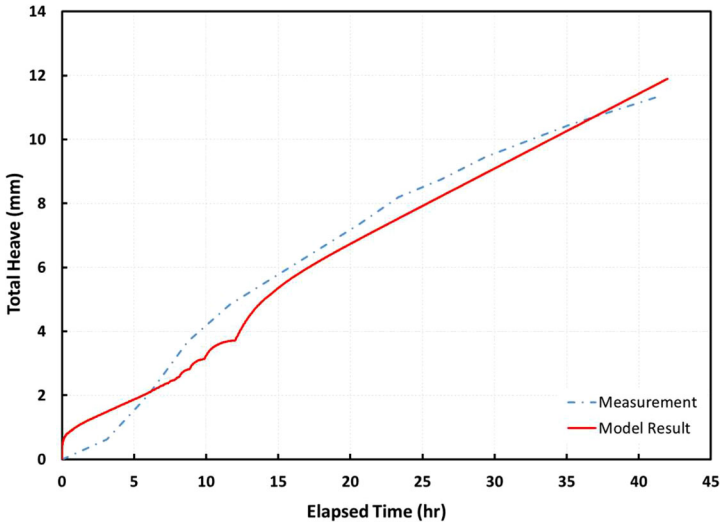

FIGURE 7 The measured (Konrad[5]) and predicted heave in sample 1 with zero overburden

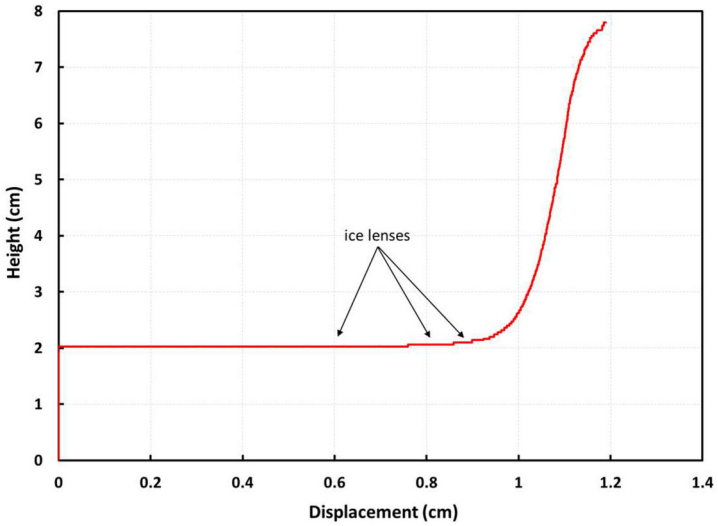

FIGURE 8 Displacement profile at the end of the test (sample 1 with zero overburden)

4.1 | Frost heave without overburden pressure

In this case (sample 1), a sample of 78 mm height and 100 mm diameter was subjected to freezing from the top surface at −5.5°C, while the bottom temperature was kept at +3°C. The sample was initially at +3°C. The duration of the test was 42 h, and water was freely available at the base at zero pressure. The surface heave history was recorded.

Figure 7 illustrates the calculated heave in comparison with the measurements, and reasonable agreement has been achieved. The displacement field at the end of the test is illustrated in Figure 8. The jumps in the displacement field represent the position and thickness of the ice lenses. As expected (see e.g., Azmatch et al.[35]), many cracks appeared in the sample, but only a few of them had the opportunity to allow an ice lens to form/grow. According to the measurement,[10] the position of the final ice lens is reported at 1.8 cm in the initial configuration (2.93 cm in the final configuration). With the presented model, we found this position at 2.02 cm.

The pore water pressure and temperature profiles are shown in Figure 9. The observed oscillation in the pore water pressure filed in the frozen area is physical. It is due to the fact that the pore water pressure at the ice lens interface should balance the overburden load (which is zero in this case), and at the same time, must develop between the ice lenses so that it can cancel the temperature-gradient-induced water flow, which is satisfactorily captured by the model.

The pore water pressure just below the freezing front was also measured and reported by Konrad and Morgenstern[10] at around −18 kPa, while the presented model has predicted it to be around −13 kPa. The difference is most likely coming from the uncertainties in the estimation of the relative permeability parameters.

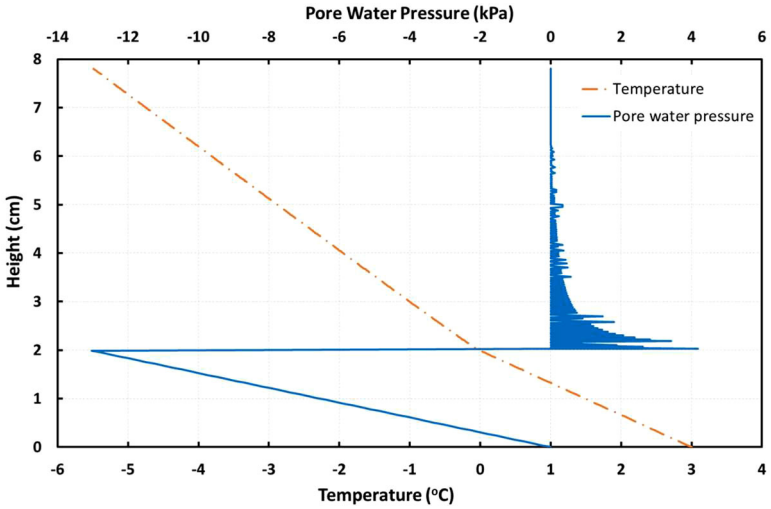

FIGURE 9 Pressure and temperature profiles at the end of the test (sample 1 with zero overburden)

TABLE 2 Simulation results and measurements for tests 2 and 3

	Measurement[5]		Simulation	
	Test 2	Test 3	Test 2	Test 3
Pore water pressure (frozen fringe base) (kPa)	−3.4	−6.5	−1.9	−4.3
Final ice lens position (initial configuration) (cm)	2.02	1.07	1.99	1.19

4.2 | Effect of overburden pressure

In this part, two frost heave tests on Devon silt samples (with the same parameters given in Table 1) under different overburden pressures and thermal boundary conditions are simulated for further validation of the model. In the first test (sample 2), a sample with 100 mm height and 100 mm diameter was subjected to freezing from the top surface at −4.7°C, while the bottom temperature was kept at +1.8°C. The overburden load for this case was 100 kPa, and the duration of the test was 141 h. In the second test (sample 3), a sample of 77 mm length and 100 mm diameter was subjected to freezing from the top surface at −3.7°C, while the bottom temperature was kept at +1°C. The overburden load for this case was 45 kPa, and the duration of the test was 42 h. Water was freely available at the base of the samples at zero pressure.

Simulation results are shown in Figures 10 and 11. As it is seen from the figures, the simulated heave has a reasonable agreement with the test results. The simulation results, in terms of pore water pressure at the base of the frozen fringe, and the position of the final ice lens in their initial configurations, are compared with the measurements, in Table 2. Ice lens positions show a good agreement with the test data. The pore water pressure shows the same trend with the experiments; we believe that the involved error originates from uncertainties in the relative permeability estimation. Figure 12 illustrates the predicted ice lens distribution in the tests. In the early stage of the tests, although the cracks form, the freezing front penetrates rapidly (as a result of large temperature gradient in the system), thus the relative permeability decreases quite rapidly, and consequently, there is no sufficient time for the formation of thick ice lenses. Advancement of the freezing front towards the warm side will decrease the temperature gradient and the frost penetration rate, as a consequence thicker ice lenses with greater spacing form progressively in the samples, as expected.

4.3 | Estimation of shut-off pressure

The minimum of the overburden pressure that is needed to stop the water intake is known as shut-off pressure.[36] The shut-off pressures for the soil samples used in Sections 4.1 and 4.2, were calculated by the proposed model. They were calculated using a trial-and-error procedure, by varying the overburden pressure to meet the necessary conditions for the shut-off pressure. This is defined at zero water intake, i.e., zero pressure gradient in the unfrozen area, where the coupling coefficient is always zero. Figure 13 shows the predicted pore water pressure profile in the samples under the estimated shut-off pressures. For the soil sample under the thermal and hydraulic boundary conditions of test 1, a shut-off pressure of about 1000 kPa was calculated by the presented model. The shut-off pressures for tests 2 and 3 were both predicted to

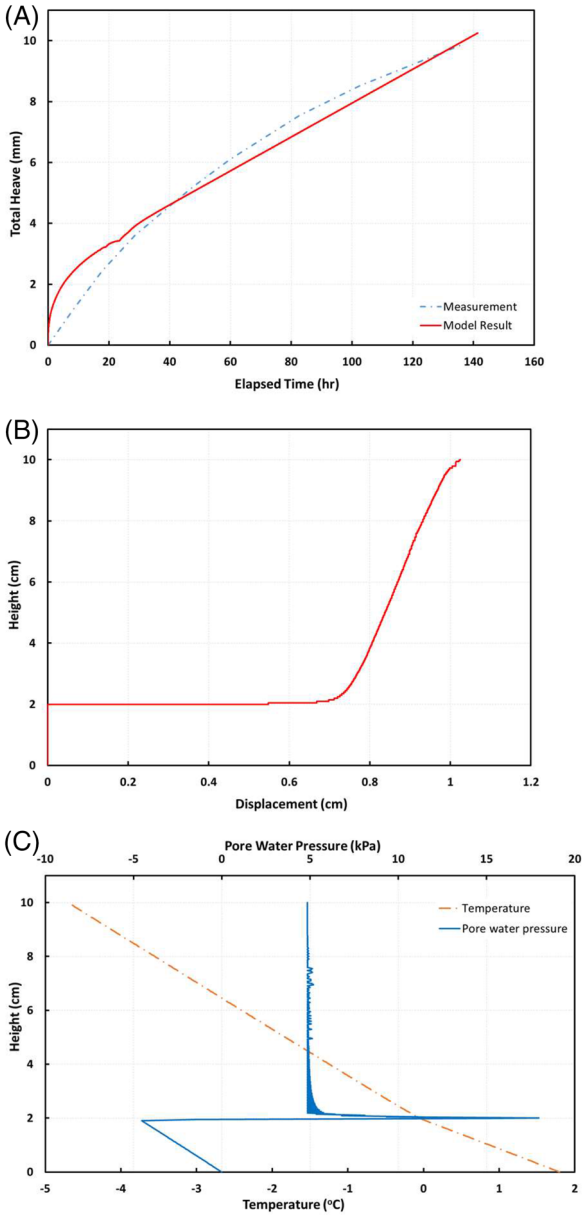

FIGURE 10 Simulation results for sample 2 with 100 kPa overburden; (a) total heave compared to measurement (Konrad[5]), (b) displacement profile, (c) temperature and pore water pressure profiles

be around 800 kPa. As expected from the physics of the phenomenon, the shut-off pressure is positively correlated with temperature gradient[5] that are, in these cases, around −108, −65 and −61°C/m, respectively for tests 1–3. The two last values explain why similar shut-off pressures were found for tests 2 and 3. The shut-off pressure for Devon silt at different practical temperature gradients was experimentally estimated by Konrad[5] and reported to be between 1000 and 1200 kPa, which is close to our results.

5 | CONCLUSION

In this paper, a fully coupled THM model was presented and tailored to simulate the complex behaviour of water-saturated porous materials being exposed to freezing condition. It is an extension of the steady state model presented by Kjelstrup et al.[18] to a transient model trough the incorporation of poromechanics. The model framework was based on a fully coupled formulation where the pore pressure, temperature, stress, displacement, heat and mass transports and unfrozen

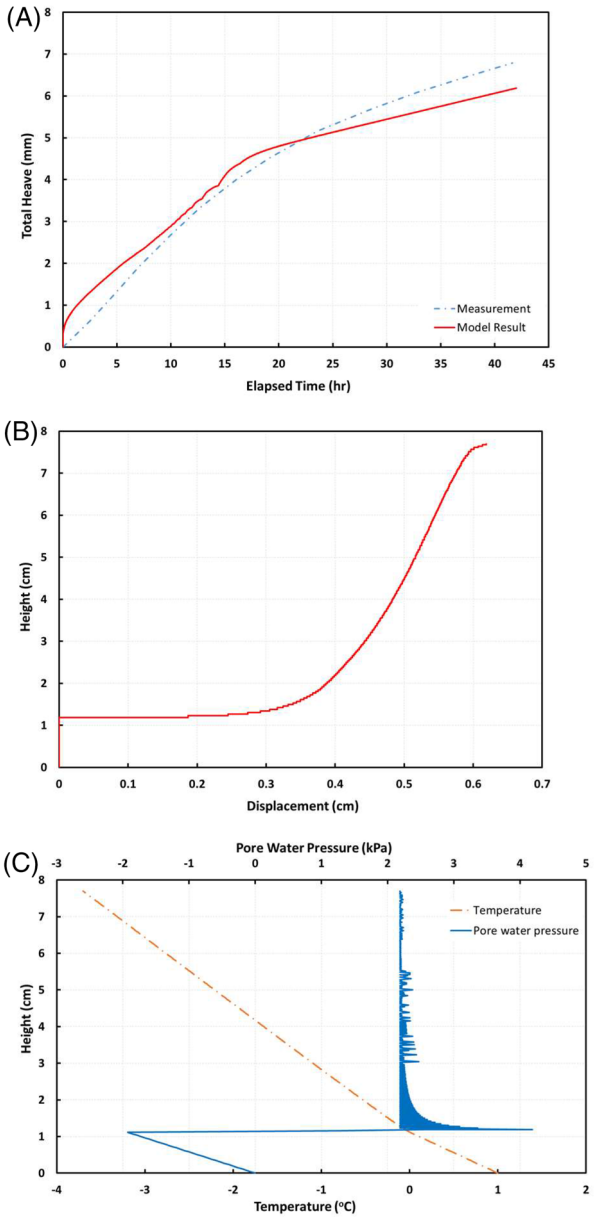

FIGURE 11 Simulation results for sample 3 with 45 kPa overburden; (a) total heave compared to measurement (Konrad[5]), (b) displacement profile, (c) temperature and pore water pressure profiles

water content are interweaved to each other. The proposed model was then numerically implemented to simulate a set of laboratory tests on Devon silt at different thermal boundary conditions and overburden pressures. The model capabilities were evaluated through a comparison with the experimental observations of total heave, pore water pressure, final ice lens position and shut-off pressure.

The following conclusions are made:

1. The coupled transport coefficient introduced by Kjelstrup et al.[18] are valid for both transient and steady state conditions. It was used in this study to simulate the whole period of frost heaving tests, that is, during both transient and steady state periods, and reasonable results were found.
2. Simulation results showed, aligned with the experimental observations, that the thickness of the ice lenses and their distancing increase toward the warm side of the experiments. The temperature dependency of the coupled transport coefficient is the key element of the model to capture this phenomenon.

FIGURE 12 Predicted ice lens distribution

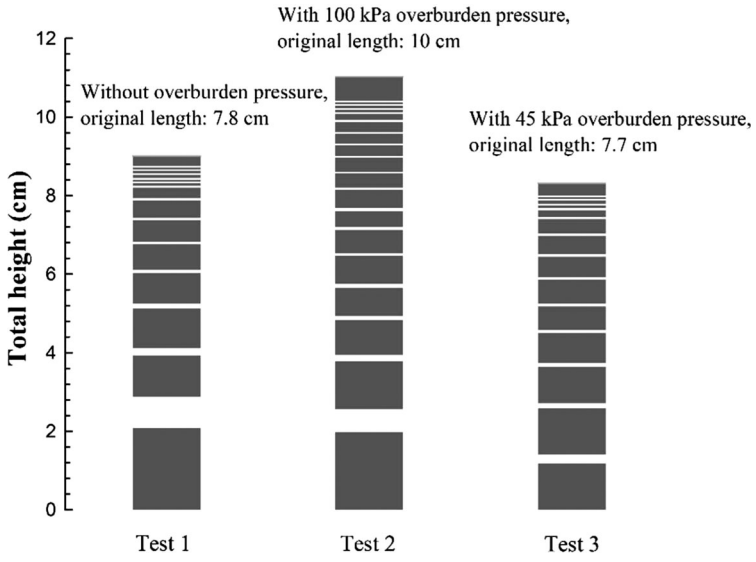

FIGURE 13 Pore water pressure profiles at the estimated shut-off pressures

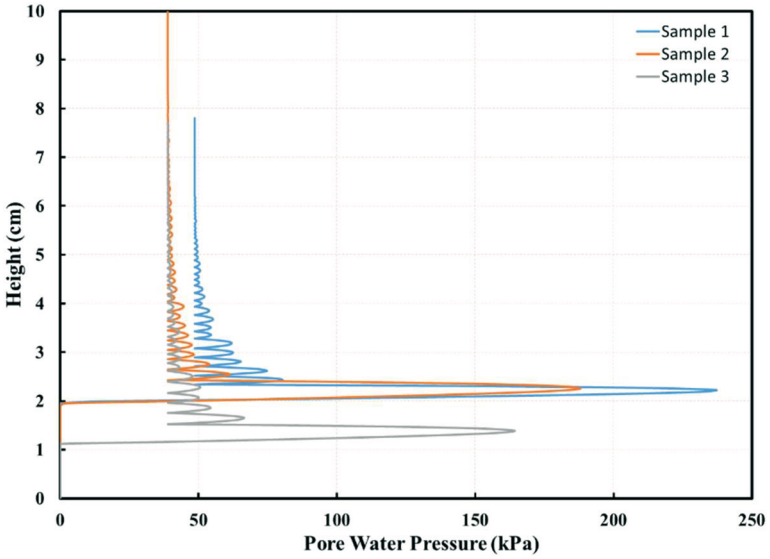

3. Considering the material discontinuities imposed by the formation of ice lenses in the system, it is more convenient to integrate the governing equations over a discontinuous solution domain. In this paper, an X-FE solution was introduced for this purpose.
4. The effect of overburden pressure on the frost heave rate was considered in the proposed model through an increase of the pore water pressure that is locally needed at the segregated area to satisfy the force equilibrium. It produces a pressure gradient which according to the coupled mass transport equation alters the mass flux of water towards the ice lens. The idea was verified by simulating a series of frost heave tests on Devon silt samples at different overburden pressure (from zero up to shut-off pressure) and reasonable agreement was achieved using a single set of parameters.

ACKNOWLEDGEMENT

This work is supported by the Research Council of Norway through its Centers of Excellence funding scheme, project number 262644 Porelab, and through Frost Protection of Roads and Railways project (FROST) under Grant Number 246826.

DATA AVAILABILITY STATEMENT

All the used data were cited, and the relevant references can be found in the reference list. Code availability: The in-house code used for solving the equations is available upon request.

ORCID

Seyed Ali Ghoreishian Amiri https://orcid.org/0000-0003-3765-246X
Gustav Grimstad https://orcid.org/0000-0003-4433-2659

REFERENCES

1. Nansen F. *Reiser gjennom Sibirien*. Jacob Dybwads forlag; 1914.
2. Rempel AW, Wettlaufer JS, Worster MG. Premelting dynamics in a continuum model of frost heave. *J Fluid Mech*. 2004;498:227-244.
3. Derjaguin BV, Churaev NV. Flow of nonfreezing water interlayers and frost heaving. *Prog Surf Sci*. 1993;43(1):232-240.
4. Zhou G-q, Zhou Y, Hu K, Wang Y-j, Shang X-y. Separate-ice frost heave model for one-dimensional soil freezing process. *Acta Geotech*. 2018;13(1):207-217.
5. Konrad J-M. *Frost Heave Mechanics*. PhD Dissertation, Department of Civil Eng., The Univ. Alberta; 1980.
6. Penner E. Aspects of ice lens growth in soils. *Cold Reg Sci Technol*. 1986;13(1):91-100.
7. Williams PJ, Riseborough DW, Smith MW. The France-Canada joint study of deformation of an experimental pipe line by differential frost heave. Int J Offshore Polar Eng. 1993;3(01):5.
8. Konrad J-M, Morgenstern NR. A mechanistic theory of ice lens formation in fine-grained soils. *Can Geotech J*. 1980;17(4):473-486.
9. Konrad J-M, Morgenstern NR. Prediction of frost heave in the laboratory during transient freezing. *Can Geotech J*. 1982;19(3):250-259.
10. Konrad J-M, Morgenstern NR. The segregation potential of a freezing soil. *Can Geotech J*. 1981;18(4):482-491.
11. Nishimura S, Gens A, Jardine RJ, Olivella S. THM-coupled finite element analysis of frozen soil: formulation and application. *Géotechnique*. 2009;59(3):159-171.
12. Zhang Y, Michalowski RL. Thermal-hydro-mechanical analysis of frost heave and thaw settlement. *J Geotech Geoenviron Eng*. 2015;141(7):04015027.
13. Ghoreishian Amiri SA, Grimstad G, Aukenthaler M, Panagoulias M, Brinkgreve RBJ, Haxaire A. *The Frozen and Unfrozen Soil Model*. Technical report – PALXIS bv; 2016.
14. Rostami H, Ghoreishian Amiri SA, Grimstad G. Back analysis of Caen's test by the recently developed frozen/unfrozen soil. *Plaxis Bull*. 2017;41:12-19.
15. O'Neill K, Miller RD. Exploration of a rigid ice model of frost heave. *Water Resour Res*. 1985;21(3):281-296.
16. Rempel AW. Formation of ice lenses and frost heave. *J Geophys Res: Earth Surf*. 2007;112:F02S21. https://doi.org/10.1029/2006JF000525
17. Rempel AW. Frost heave. *J Glaciol*. 2010;56(200):1122-1128.
18. Kjelstrup S, Ghoreishian Amiri SA, Loranger B, Gao H, Grimstad G. Transport coefficients and pressure conditions for growth of ice lens in frozen soil. *Acta Geotech*. 2021;16(7):2231-2239.
19. Ghoreishian Amiri SA, Grimstad G, Gao H, Kjelstrup S. Numerical modelling of distinct ice lenses in frost heave. *IOP Conf Ser: Earth Environ Sci*. 2021;710(1):012039.
20. Konrad J-M. Frost susceptibility related to soil index properties. *Can Geotech J*. 1999;36(3):403-417.
21. Holten GJ. *Measuring Negative Pore Pressures in Partially Frozen Saturated Soils*. MSc Thesis, Department of Civil and Environmental Engineering, NTNU; 2017.
22. Thomas HR, Harris C, Cleall P, Kern-Luetschg M, Li YC. Modelling of cryogenic processes in permafrost and seasonally frozen soils. *Géotechnique*. 2009;59(3):173-184.
23. Ghoreishian Amiri SA, Taheri E, Lavasan AA. A hybrid finite element model for non-isothermal two-phase flow in deformable porous media. *Comput Geotechn*. 2021;135:104199.
24. Ghoreishian Amiri SA, Grimstad G, Kadivar M, Nordal S. Constitutive model for rate-independent behavior of saturated frozen soils. *Can Geotech J*. 2016;53(10):1646-1657.
25. Watanabe K, Osada Y. Comparison of hydraulic conductivity in frozen saturated and unfrozen unsaturated soils. *Vadose Zone J*. 2016;15(5):1-7.
26. van Genuchten MT. A closed-form equation for predicting the hydraulic conductivity of unsaturated soils1. *Soil Sci Soc Am J*. 1980;44:892-898.
27. Kurylyk BL, Watanabe K. The mathematical representation of freezing and thawing processes in variably-saturated, non-deformable soils. *Adv Water Res*. 2013;60:160-177.
28. Førland T, Kjelstrup Ratkje S. Irreversible thermodynamic treatment of frost heave. *Eng Geol*. 1981;18(1):225-229.
29. Konrad J-M, Morgenstern NR. Effects of applied pressure on freezing soils. *Can Geotech J*. 1982;19(4):494-505.
30. Konrad J-M. Estimation of the segregation potential of fine-grained soils using the frost heave response of two reference soils. *Can Geotech J*. 2005;42(1):38-50.
31. Mohammadnejad T, Khoei AR. An extended finite element method for hydraulic fracture propagation in deformable porous media with the cohesive crack model. *Finite Elem Anal Des*. 2013;73:77-95.
32. Khoei AR. *Extended Finite Element Method: Theory and Applications*. John Wiley & Sons, Ltd.; 2014.
33. Moës N, Cloirec M, Cartraud P, Remacle JF. A computational approach to handle complex microstructure geometries. *Comput Meth Appl Mech Eng*. 2003;192(28):3163-3177.
34. Azmatch TF. Frost Heave: New Ice Lens Initiation Condition and Hydraulic Conductivity Prediction. *PhD thesis*. Department of Civil and Environmental Engineering, University of Alberta; 2013.

35. Azmatch TF, Sego DC, Arenson LU, Biggar KW. Tensile strength and stress–strain behaviour of Devon silt under frozen fringe conditions. *Cold Reg Sci Technol*. 2011;68(1):85-90.
36. Arvidson WD, Morgenstern NR. Water flow induced by soil freezing. *Can Geotech J*. 1977;14(2):237-245.

How to cite this article: Gao H, Ghoreishian Amiri SA, Kjelstrup S, Grimstad G, Loranger B, Scibilia E. Formation and growth of multiple, distinct ice lenses in frost heave. *Int J Numer Anal Methods Geomech*. 2022;1-24. https://doi.org/10.1002/nag.3461

APPENDIX A

The coefficient matrices in Equation (63) are listed below:

$$\mathbf{C}_{up}^{\text{std-}\beta} = -\int_{\Omega} s_w \left(\mathbf{B}_u^{\text{std}}\right)^T \mathbf{N}_p^{\beta} \mathbf{I} d\Omega \tag{A1}$$

$$\mathbf{C}_{up}^{\text{enr-}\beta} = -\int_{\Omega} s_w (\mathbf{B}_u^{\text{enr}}\mathbf{L})^T \mathbf{N}_p^{\beta} \mathbf{I} d\Omega \tag{A2}$$

$$\mathbf{Q}_{pp}^{\alpha\text{-}\beta} = \int_{\Omega} \left(\mathbf{B}_p^{\alpha}\right)^T \frac{k_r K}{\mu_w} \rho_w \mathbf{B}_p^{\beta} d\Omega \tag{A3}$$

$$\mathbf{C}_{pT}^{\alpha\text{-}\beta} = \int_{\Omega} \left(\mathbf{B}_p^{\alpha}\right)^T \alpha \frac{k_r K}{\mu_w} \frac{\rho_i l}{T} \rho_w \mathbf{B}_T^{\beta} d\Omega \tag{A4}$$

$$\bar{\mathbf{C}}_{pu}^{\alpha\text{-std}} = \int_{\Omega} \left(\mathbf{N}_p^{\alpha}\right)^T \left(s_w \rho_w + s_i \rho_i\right) \mathbf{m}^T \mathbf{B}_u^{\text{std}} d\Omega \tag{A5}$$

$$\bar{\mathbf{C}}_{pu}^{\alpha\text{-enr}} = \int_{\Omega} \left(\mathbf{N}_p^{\alpha}\right)^T \left(s_w \rho_w + s_i \rho_i\right) \mathbf{m}^T \mathbf{B}_u^{\text{enr}} \mathbf{L} d\Omega \tag{A6}$$

$$\bar{\mathbf{C}}_{pT}^{\alpha\text{-}\beta} = \int_{\Omega} \left(\mathbf{N}_p^{\alpha}\right)^T \left[n\left(\rho_w - \rho_i\right) \frac{\partial s_w}{\partial T} + \chi\right] \mathbf{N}_T^{\beta} d\Omega \tag{A7}$$

$$\mathbf{C}_{Tp}^{\alpha\text{-}\beta} = \int_{\Omega} \left(\mathbf{B}_T^{\alpha}\right)^T \alpha \frac{k_r K}{\mu_w} \rho_i l \mathbf{B}_p^{\beta} d\Omega \tag{A8}$$

$$\mathbf{H}_{TT}^{\alpha\text{-}\beta} = \int_{\Omega} \left(\mathbf{N}_T^{\alpha}\right)^T \left(\rho_w C_w \mathbf{q}_w\right) \mathbf{B}_T^{\beta} d\Omega + \int_{\Omega} \left(\mathbf{B}_T^{\alpha}\right)^T \left(\lambda_s^{1-n} . \lambda_w^{n s_w} . \lambda_i^{n s_i}\right) \mathbf{B}_T^{\beta} d\Omega \tag{A9}$$

$$\bar{\mathbf{H}}_{TT}^{\alpha\text{-}\beta} = \int_{\Omega} \left(\mathbf{N}_T^{\alpha}\right)^T (\rho C)_{\text{eff}} \mathbf{N}_T^{\beta} d\Omega \tag{A10}$$

where $(\alpha, \beta) \in (\text{std}, \text{enr})$ denote the standard and enriched parts of the field variables and shape functions.

Indeed, the internal and external load vectors are listed below:

$$^{\text{int}}\mathbf{F}_u^{\text{std}} = \int_{\Omega} \left(\mathbf{B}_u^{\text{std}}\right)^T \boldsymbol{\sigma}^* d\Omega \tag{A11}$$

$$^{\text{int}}\mathbf{F}_u^{\text{enr}} = \int_{\Omega} (\mathbf{B}_u^{\text{enr}}\mathbf{L})^T \boldsymbol{\sigma}^* d\Omega + \int_{\Gamma_d} (\bar{\mathbf{N}}_u \mathbf{L})^T . \left(\beta_2 s_{i_d} + 1\right) \left(p_w \mathbf{I}\right)_d \mathbf{n}_{\Gamma_d} d\Gamma \tag{A12}$$

$$^{\text{ext}}\mathbf{F}_u^{\text{std}} = \int_{\Gamma_t} \left(\mathbf{N}_u^{\text{std}}\right)^T \bar{\mathbf{t}} d\Gamma + \int_{\Omega} \left(\mathbf{N}_u^{\text{std}}\right)^T \rho \mathbf{g} d\Omega \tag{A13}$$

$$^{\text{ext}}\mathbf{F}_u^{\text{enr}} = \int_{\Gamma_t} (\mathbf{N}_u^{\text{enr}}\mathbf{L})^T \bar{\mathbf{t}} d\Gamma + \int_{\Omega} (\mathbf{N}_u^{\text{enr}}\mathbf{L})^T \rho \mathbf{g} d\Omega \tag{A14}$$

$$^{\text{int}}\mathbf{F}_p^{\alpha} = \int_{\Gamma_d} \left(\mathbf{N}_p^{\alpha}\right)^T \rho_w \bar{q}_{w_d} d\Gamma \tag{A15}$$

$$^{\text{ext}}\mathbf{F}_p^{\alpha} = \int_{\Omega} \left(\mathbf{B}_p^{\alpha}\right)^T \frac{k_r K}{\mu_w} \rho_w \left(\rho_w \mathbf{g}\right) d\Omega - \int_{\Gamma_{q_w}} \left(\mathbf{N}_p^{\alpha}\right)^T \rho_w \bar{q}_w d\Gamma \tag{A16}$$

$$^{\text{int}}\mathbf{F}_T^{\alpha} = \int_{\Omega} \left(\mathbf{N}_T^{\alpha}\right)^T l \dot{m}_{w\to i} d\Omega + \int_{\Gamma_d} \left(\mathbf{N}_T^{\alpha}\right)^T \bar{q}_{H_d} d\Gamma \tag{A17}$$

$$^{\text{ext}}\mathbf{F}_T^{\alpha} = \int_{\Omega} \left(\mathbf{B}_T^{\alpha}\right)^T \alpha \frac{k_r K}{\mu_w} \rho_i l (\rho_w \mathbf{g}) d\Omega - \int_{\Gamma_{q_H}} \left(\mathbf{N}_T^{\alpha}\right)^T \bar{q}_H d\Gamma \tag{A18}$$